THE OPTICAL EFFECTS OF TEAR FILM DISRUPTION

BY

RONALD COGSWELL TUTT

Submitted to the Faculty of the University Graduate School

in partial fulfillment of the requirement

for the degree

Master of Science in Physiological Optics

in the Department of Physiological Optics
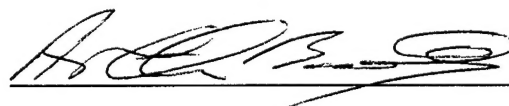
Indiana University

February 1999

REPORT DOCUMENTATION PAGE

1. AGENCY USE ONLY (Leave blank)	2. REPORT DATE	3. REPORT TYPE AND DATES COVERED
	13.May.99	THESIS

4. TITLE AND SUBTITLE
THE OPTICAL EFFECTS OF TEAR FILM DISRUPTION

5. FUNDING NUMBERS

6. AUTHOR(S)
MAJ TUTT RONALD C

7. PERFORMING ORGANIZATION NAME(S) AND ADDRESS(ES)
INDIANA UNIVERSITY BLOOMINGTON

8. PERFORMING ORGANIZATION REPORT NUMBER

9. SPONSORING/MONITORING AGENCY NAME(S) AND ADDRESS(ES)
THE DEPARTMENT OF THE AIR FORCE
AFIT/CIA, BLDG 125
2950 P STREET
WPAFB OH 45433

10. SPONSORING/MONITORING AGENCY REPORT NUMBER

FY99-107

11. SUPPLEMENTARY NOTES

12a. DISTRIBUTION AVAILABILITY STATEMENT
Unlimited distribution
In Accordance With AFI 35-205/AFIT Sup 1

12b. DISTRIBUTION CODE

13. ABSTRACT (Maximum 200 words)

14. SUBJECT TERMS

15. NUMBER OF PAGES

16. PRICE CODE

17. SECURITY CLASSIFICATION OF REPORT	18. SECURITY CLASSIFICATION OF THIS PAGE	19. SECURITY CLASSIFICATION OF ABSTRACT	20. LIMITATION OF ABSTRACT

Accepted by the Graduate Faculty, Indiana University, in partial fulfillment of the requirements for the degree Master of Science.
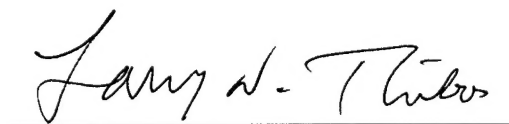
Arthur Bradley, PhD.

Chairman of the Committee

Carolyn G. Begley, OD, MS

Lawrence N. Thibos, PhD.

ACKNOWLEDGMENTS

TABLE OF CONTENTS

TABLES

FIGURES

INTRODUCTION

The most anterior optical surface of the eye has the greatest refractive power. Therefore, the quality of this surface is critical to retinal image quality and visual performance. Most optical texts identify the cornea as the first optical surface [1, 2, 3, 4, 5], but in fact it is the tear layer [6, 7, 8, 9, 10, 11, 12]. A smooth tear layer is considered optically essential and superior to the microscopically irregular corneal epithelium [8, 12, 13, 14]. Unlike the other optical surfaces within the eye, the tear film can vary tremendously from second to second as tear film changes occur between blinks [6, 9, 15, 16, 17, 18, 19, 20, 21, 22, 23, 24, 25, 26, 27, 28, 29, 30]. Although numerous studies have evaluated the change in tear film "quality" during periods of non-blinking [6, 7, 16, 18, 19, 20, 21, 22, 24, 26, 27, 28, 31, 32, 33, 34, 35, 36, 37, 38] little is known about the optical and visual effects resulting from changes in the tear film layer [9, 12, 39].

The classic tear film models suggest that the precorneal tear film is composed of three layers [2, 6, 7, 13, 14, 40, 41, 42, 43]; the superficial lipid layer derived from the meibomian glands, the middle aqueous layer provided by the major and minor lacrimal glands maintains ocular wetting, among other physiological effects, and the inner most layer overlies the corneal and conjunctival epithelial cells with mucous like material. Recent studies suggest that the tear film is composed of a mucin "gel" topped by a thin lipid film [40, 41, 43, 44, 45].

Although in most people the tear film is considered stable, it's well known that the tear film will eventually break-up [6, 7, 9, 13, 14, 16, 19, 20, 21, 24, 25, 27, 28, 29, 33, 34, 37, 38, 40,

[41, 46]. However, the mechanism of tear film disruption is controversial [6, 18, 21, 28, 29, 33, 37, 38, 40, 41]. Classic studies by Holly and Padday demonstrated that an aqueous structure like the tear film will spontaneously disrupt once the supporting surface becomes hydrophobic [6, 7, 47]. Some studies have suggested that tear film disruption is the result of increasing lipid contamination (bubbles, dust particles, airborne chemicals, etc.) secondary to tear film thinning [6, 7, 8, 14, 15, 35]. Alternatively, Fatt and others suggest that tear film disruption occurs when the tension created by the curved tear film surface at the lower lid margin becomes greater than the tensile strength of the tear film [15, 37, 41, 47].

The clinical impact of tear film quantity and quality has been studied extensively in "dry eye" subjects and contact lens wearers [2, 3, 8, 15, 17, 20, 22, 23, 25, 26, 27, 31, 34, 35, 37, 41, 47, 48]. Studies suggest that the introduction of soft or rigid contact lenses on the corneal surface will alter the tear film characteristics [12, 14, 23, 39, 48, 49]. Evaluation and diagnosis of tear film anomalies, including its disruptions over the corneal surface have been studied by a variety of methods [2, 3, 17, 19, 21, 22, 25, 28, 31, 32, 34, 44, 45].

Holly grouped current "dry eye" diagnostic methods into four categories: clinical presentation, tear related, tear film related, and ocular surface related (appendix 1) [22]. Diagnosis by clinical presentation is based on subjective complaint and gross observation typically performed with a biomicroscope examination. Examination of tear related components includes an evaluation of the secretion rate, osmolality, mucous ferning, tear cytology, protein content, or enzymatic activity. The tear film methods generally examine the break-up time, evaporation rate, or the lipid spreading ability. Finally, methods of ocular surface evaluation focus on cytology and microscopy of the ocular

2

tissues. However, none of these methods relate tear film dynamics to the optical and visual impact of its disruption.

Most researchers accept the presence of a relationship between tear film dynamics and the tear film's impact on the optical quality of the eye. The majority of the accepted models of tear film disruption predict a change in optical quality [15, 37, 41, 45, 47, 50, 51]. These models suggest local structural changes in tear film may be caused directly by local surface tension or by the result of aqueous gaps caused by the lipid layer's attraction to the mucin as the tear film thins. Regardless of the etiology, structural disruption of the optically smooth tear film surface introduces optical discontinuities, which in turn lead to increases in light scatter or high order aberrations. With increasing light scatter, image quality and contrast sensitivity measures decline [50, 52, 53, 54, 55, 56, 57, 58, 59, 60]. Although this relationship is recognized, changes in the anterior refracting surface and its optical impact have been rarely investigated.

To date three studies have reported an association of tear film quality to visual or optical performance. Rieger et al reported improved visual field perimetery results in dry eye subjects when pretreated with tear supplements [9]. Timberlake et al found a reduction in low contrast small letter acuity associated with prolonged periods of non-blinking in soft contact lens wearers [12]. In a recent study by Albarran et al [61], used modulation transfer function (MTF) measures to evaluate changes in optical quality after tear break-up. They determined that measurable optical quality loss could be attributed to tear film disruption. Together, these studies support the hypothesis that disruptions or changes in

3

the optical characteristics of the tear film will result in a degradation of visual performance.

Of these three studies, only Albarran's technique used objective measures of optical quality changes. Rieger's and Timberlake's studies employed subjective methods that are difficult to quantify. However, Albarran's technique did not allow for multiple sequential measures over each individual tear film disruption. We developed a video-based method to acquire continuous real-time data to enable continuous measures of optical and tear film changes during a period of non-blinking.

We employed objective computerized techniques for fundus image analysis to study the impact of tear film disruption. Previous studies using objective computer analysis have been directed at pattern recognition or intensity based algorithms to assist in retinal disease diagnosis, or digital subtraction techniques used in angiogram studies [62, 63, 64]. Computer analysis techniques have also been implemented to evaluate the optic disk in glaucomatous conditions [65]. To the author's knowledge, there have been no studies using computer analysis to examine changes in fundus images associated with tear film disruption.

In the present study we have (1) developed a novel objective method for quantifying tear film disruption and (2) examined the optical and visual impact of tear film disruptions.

For the test procedures described below, data was collected on three subjects. Each subject had the test eye cyclopleged OS (1% cyclopentolate, 1-2 drops) prior to acquisition. Additionally, the non-tested eye (OD) was fit with a group 4 high water content soft contact lens (SCL) to provide the ocular surface comfort and protection during the test period. Data was collected under two experimental conditions. In the first experiment (Exp 1), the test eye was fit with group 4 ionic high water SCL allowing the examination of tear film disruption over a SCL material. The second experimental condition (Exp 2) examined tear film disruption over the uncovered cornea (no SCL applied to the test eye). Prior to data acquisition under this second condition, the test eye was anesthetized (1-2 drops, 0.5% proparacaine OS) to minimize reflex tearing and maintain subjective comfort.

Both experimental paradigms included psychophysical and physical measures of optical, visual and tear film quality. The order of experimental conditions and data acquisition was randomized for each subject. Although desirable, our experimental design did not allow for simultaneous acquisition of various measures. To minimize residual tear film and accumulative corneal effects, each condition was acquired on a separate day.

Retinal vessel contrast (RVC) data were derived from fundus images acquired using a video biomicroscope (Zeiss 20 SL) and a clear +90 Diopter fundus lens (Volk). The biomicroscope magnification was set at 20x for all fundus image acquisitions. The

+90 Diopter lens was aligned and stabilized on the optic disk using a standard lens holder (Volk). The retinal area illuminated by the biomicroscope light source was approximately 15 x 20 degrees centered on the vessel rich area surrounding and within the optic disk. Illumination was adjusted to provide a balance between the maximal brightness contrast, and subject comfort to prevent reflexive tearing. Additionally, the first Purkinje image was decentered as much as possible. The subject was positioned and stabilized using a standard biomicroscope headrest. Prior to each acquisition, the subject was instructed to blink three to four times, fixate using the non-tested eye on an external stimulus and suspend blinking as long as possible. Fundus images were recorded at normal video rate on high definition videotape (S-VHS).

Fundus images were captured with a high resolution CCD video camera (Sony DXC-107AP) and recorded at 30 frames / second (standard NTSC signal) on a S-VHS video recorder (Mitsubishi HS-U69). The standard NTSC protocol dictates a video image resolution to be 720 x 486 pixels (picture elements). Fundus video images were digitized using Avid VideoShop® 3.0.2 on an Apple 7500/100 PowerMac® into sequential 640x480 pixel arrays selecting one frame/second. Further processing of these digitized fundus images was accomplished using macro programming (appendix 3) within an image processing program (NIH-Image version 1.60, available through: (http://rsb.info.nih.gov/nih-image/). The sequence of images from each trial was spatially aligned. Vessel intensity profiles (figure 1) were developed for each image in each series. Figures 2 and 3 present examples of the video fundus images captured in Exp 2 and 1. Local vessel contrast values were determined using Weber's definition [54] "(delta L)/L"

from the intensity profiles. The contrast values for the three vessel locations in each series were averaged and normalized for comparison to the psychophysical data.

Psychophysical contrast sensitivity (CS) data were collected utilizing a Pelli-Robson chart (figure 4) set at a test distance of two meters. This distance was selected to create a letter stroke width (17 arc minutes) that approximated the average vessel diameter (18 arc minutes) used in the fundus video images. Each subject was provided with the appropriate over-refraction for acquisition of the CS data. The non-tested eye (OD) was covered with an eye patch. Prior to each timed trial, the minimum visible letter group was reported and recorded. Minimum visible letter group for this study was considered the lowest contrast in which all three letters within a contrast group were recognizable. Subjects were then instructed to blink three to four times, and hold their eyes open as long as possible. During this period of non-blinking, subjects would fixate on the minimum visible letter group, report loss of readability and then refixate on the next recognizable letter group. This process continued until terminated by the subjects first blink. The progression of contrast steps (letter groups) and the corresponding elapsed time was recorded.

For video imaging of the retro-illuminated tear film, the subject was positioned at the biomicroscope in the same manner used in the fundus imaging protocol. The biomicroscope illumination was positioned to produce maximal retro-illumination of the tear film, without stimulating reflexive tearing. The subject was directed to blink three to four times, fixate with the non-tested eye on an external light source and hold their eyes

open as long as possible. During this period of non-blinking, video rate images of the tested eye were captured on high definition videotape for later display and analysis.

RESULTS

Retinal Vessel Contrast:

All subjects under both experimental conditions demonstrated a decrement in retinal vessel contrast (RVC) immediately following the suspension of a blink. Although individual trials were variable, all subjects followed a similar trend under both paradigms (figures 5 and 6). The averaged data from the "with SCL" condition was very similar in both the rate and amount of contrast reduction. As figure 7 presents, one subject (rt) consistently demonstrated less contrast loss than the other two subjects during Exp 1 (without SCL). However, with the exception of that data set, the other data sets from Exp 1 and 2 were all similar. The overall averages under each experimental condition representing all retinal vessel contrast trials are summarized in table 1.

Table 1

RETINAL VESSEL CONTRAST

Average Percent Reduction from Baseline

RVC Paradigm	@ 10 sec	@ 20 sec	@ 30 sec	@ 40 sec	@ 50 sec	@ 60 sec
Exp 1 (with SCL)	10% ±13	18% ±17	32% ±14	37% ±14	46% ±13	59% ±7
Exp 2 (w/o SCL)	7% ±9	25% ±15	39% ±21	55% ±21	55% ±14	62% ±16

Contrast Sensitivity:

Consistent with the RVC data sets, both experimental CS conditions demonstrated a decrease in CS beginning after a blink observed by all subjects in all trials. As found with the RVC trials, individual CS trials were variable in the time course and amount of contrast loss under each condition (figure 8 and 9). There was, however, a consistent pattern within each subject's data. Although contrast sensitivity reductions were similar with and without SCLs, the presence of a SCL led to slightly more loss of contrast sensitivity (figure 10). The overall averages under each paradigm of all contrast sensitivity trials are summarized in table 2.

Table 2

CONTRAST SENSITIVITY

Average Percent Reduction from Baseline

CS Paradigm	@ 10 sec	@ 20 sec	@ 30 sec	@ 40 sec	@ 50 sec	@ 60 sec
Exp 1 (with SCL)	20% ±16	54% ±18	67% ±19	69% ±19	68% ±15	76% ±18
Exp 2 (w/o SCL)	12% ±16	33% ±12	42% ±16	47% ±7	50% ±9	52% ±10

Comparison of Retinal Vessel Contrast to Contrast Sensitivity Data:

Figure 11 compares the average RVC and CS data under each experimental condition. As noted above, the CS data with SCL revealed a slightly more rapid and overall greater loss of contrast than without SCL. The other three conditions were remarkably similar.

Retro-illumination of the Tear Film:

Videotaped retro-illuminated tear film images were examined for patterns and trends. Following the suspension of blinking, a pattern of tear film disruption developed. The foci of disruption began in various locations, typically within the lower to middle third of the retro-illuminated image. From this initial location or adjacent to it, a pattern of disruption expanded in the form of vertical "rivulets" appearing as rod shaped or branching patterns increasing toward superior cornea. Some of these formations coalesced, but most did not. The disruption pattern ceased to expand as soon as blinking resumed. After the initial few blinks, the original disruption pattern diminished but remained identifiable. With additional blinking and time, the original pattern became unrecognizable. With a subsequent period of non-blinking, new disruption patterns developed and spread, independent of the previous pattern development. Despite inconsistencies of the disruption initiation and development, the final retro-illuminated tear pattern for each subject under each condition throughout each trial appeared similar. This suggests an underlying geographic or physical component to tear film disruption

10

patterns. Examples of retro-illuminated tear film disruption patterns with and without SCL are presented in figures 12,13, 14, and 15.

During the acquisition of RVC and retro-illumination data, a fixation light was subjectively observed with the non-tested eye. The subjects anecdotally reported color halos appeared around the fixation light during the period of non-blinking. The size and appearance of the color halos changed in a trend similar to the contrast data. That is, fringes appeared immediately following a blink. These fringes enlarged and seemed to stabilize in size during the period of non-blinking. Upon termination of the non-blinking period, these fringes dramatically reduced in size or disappeared, mirroring the recovery of contrast or tear film uniformity.

DISCUSSION

We have developed a novel objective method for quantifying the optical effects of tear film disruption using a video based method to provide real-time data. The comparison of objective retinal vessel contrast (RVC) measurements to psychophysical contrast sensitivity measurement demonstrated a consistent pattern of optical contrast attenuation that accompanies tear film disruptions during prolonged periods of non-blinking. This supports the hypothesis that the tear film layer plays an important role in optical performance of the human eye.

The results demonstrate that disruption of the tear film directly impacts the optical performance of the eye with and without SCLs. This is consistent with the findings of

Albarran's study [61]. It is well known that both SCLs and the cornea have microscopically irregular surfaces that are neutralized or "optically smoothed" by the tears [8, 12, 13, 14]. However, it is uncertain from this study whether the decrease in optical performance during a period of non-blinking is the due to exposure of the underlying irregular surface, the irregular surface of the tear film during disruption, or a combination of both.

It has been suggested that contrast loss (Timberlake[12]) or light scattering (Lohmann[39]) associated with periods of non-blinking might be due to changes in SCL parameters (curvature, refractive indices, etc.) secondary to lens dehydration. In their studies, SCLs demonstrated much higher contrast loss than RGPs or normal cornea. We did not observe this difference in our study, but obtained very similar responses under both SCL and normal cornea conditions. Further, under both experimental conditions (with and without SCLs), all contrast measures approached the initial (immediately post blink) values within one or two blinks after long periods of non-blinking. The "with SCL" condition did, however, require slightly more time to fully return to the initial contrast than the without SCL condition, suggesting that SCL material, design and/or condition may have a differential effect on tear film equilibrium / rehydration recovery as compared to the cornea. The difference in recovery may also be attributed to different mechanisms of disruption under the two conditions.

It was expected that individual physiology would result in variable tear film breakup or disruption patterns [6, 7, 8, 9, 10, 11, 12, 15, 16, 17, 18, 19, 20, 22, 23, 24, 25, 26, 27, 28, 29, 30]. As previously described, the tear film is subject to continuous changes in its composition, contaminates, and surface tension. These factors in addition to the underlying surface

12

quality, contribute to tear film disruption variability . The results showed the rate and amount of RVC and CS decrement did, indeed, vary between subjects (figures 5, 6, 8, and 9), as well as within subjects. Although variability was a factor in each trial, a subject's data from a given condition demonstrated a similar trend. All data reported for each individual experimental condition (figures 5, 6, 8, and 9) reflect the condition of the subject's eye and SCL (if used) for that day. Additionally, to minimize the residual effects of repeated periods of non-blinking on the cornea, we acquired data for each experimental condition on separate days.

Consistent with Albarran [61], we found the rate and amount of RVC change was similar (figure 11) for all eyes with and without SCL. This is in contrast to the studies of Timberlake and Lohmann [12, 39] that compared SCL and rigid gas permeable lens (RGP) to the uncovered cornea and found that eyes with SCLs were affected more by non-blinking than were eyes with RGPs or without contact lenses. Timberlake et al measured greater reduction in low contrast acuity with soft contact lenses. Lohmann et al observed an increase in light scattering associated with soft contact lenses. However, in both of these studies, comparative data was acquired using a psychophysical stair-step method over extended periods of time (minutes). In our study, we found that the cornea, unprotected and without anesthetic quickly became uncomfortable (within seconds). This discomfort resulted in the need to blink and/or initiated reflexive tearing which in turn refreshed or altered the degrading tear film. Control of reflexive tearing was not indicated by their reports and thus the failure to observe changes without SCLs may be a bi-product of excessive reflex tearing during the experiment.

13

Neither Timberlake nor Lohmann's studies reported control of the water content, material, age, or condition of the soft contact lenses worn by the subjects [12, 39]. These factors would certainly impact the measurement of contrast acuity changes or light scatter over SCL surface more than that of a RGP surface or a corneal surface. In our study, we attempted to minimize the impact of water content and some of the lens surface conditions, such as protein deposits, by the use of a new disposable SCL worn during the acquisition of each experimental condition and then replaced.

Retro-illuminated tear film images provided a visual demonstration of the changing characteristics of the optical surfaces (tear film, contact lens, and cornea) during periods of non-blinking. Consistent with the contrast data, disruption of the optical surface began immediately upon the suspension of blinking. The foci of the initial disruption typically appeared in the lower to middle third of the retro-illuminated area. This is consisted with the tear film break-up predictions of Fatt and others [15, 16, 37, 41]. This initial foci developed into rod-shaped or branching rivulets, rapidly spreading across the retro-illuminated image. The central optical zone was not always involved in the initial disruption. However, this area was typically encroached upon within 5-10 seconds. Between 30-60 seconds after the suspension of a blink, the spread of disruption extended to the entire retro-illuminated surface. The final pattern of disruption appeared to be similar from trial to trial for a given subject and condition. Although limited in this study to three subjects, these observations may be important for studies that isolate the central optical zone for measurements.

14

To illustrate the similarities between the retro-illuminated images and the contrast data, the following time-line description is provided. Under normal conditions and prior to the suspension of a blink, the retro-illuminated image can be described as a smooth and uniform surface, representing the optimal tear film condition. Contrast data acquired during the equivalent time frame were noted to be the "best" contrast level. Immediately following the blink the retro-illuminated image demonstrated a focal area of disruption. Similarly, contrast data acquired at time period showed a small drop in sensitivity. As the period of non-blinking progressed, areas of disruption in the retro-illuminated tear film expanded and become more defined. The corresponding contrast sensitivity declined. As the period of non-blinking continued (30 – 60 seconds), the tear film disruption stabilized into a pattern that remained until the next blink. The contrast data appeared to reach a plateau that also remained until the subsequent blink. Immediately following a blink, the area of disruption dramatically reduced or disappeared. Correspondingly, the contrast measures recovered partially or completely. Although the techniques used in this study did not allow for simultaneous acquisition of retro-illuminated images with corresponding contrast data, there was a strong consistency in the results as described.

The etiology of the contrast/image degradation is not clear. Both scatter and defocus have been suggested as possible sources. Figures 16 and 17 show the classic effects of defocus and light scattering on contrast sensitivity. Note that in figure 16, defocus decreases CS at high frequency, but the low frequencies are relatively insensitive to defocus [39, 42, 50, 53, 54, 55, 56, 58, 59, 66, 67, 68, 69]. Scatter (figure 17) may affect the contrast sensitivity at all frequencies. The video fundus images as acquired were

15

spectrally analyzed and found to contained frequencies principally around one to three cycles per degree. The letter targets of the Pelli-Robson at the distance selected have a characteristic frequency of approximately 1 cycle/degree. At these frequencies, defocus would not be expected to affect CS. For example, 3-4 diopters of defocus would be required to attenuate contrast by 70% at 1 cycle/degree with an eight millimeter pupil [70]. Therefore, the optical impact created by tear film disruption can be attributed principally to scatter or aberrations. Additionally, the retro-illuminated data acquired from both experimental conditions also supports the hypothesis that scatter is the major etiology of the tear film's optical degradation. The progression of non-uniformity over the retro-illuminated image mirrored the contrast degradation over time after withholding normal blinking. Further, both the contrast data and uniformity of the retro-illuminated images virtually returned to the initial state once blinking was allowed to re-establish the tear film. However, to properly differentiate scatter from defocus, contrast data over several spatial frequencies would be required.

The methodology of this study dictated some limitations. Foremost, this study's design did not allow simultaneous acquisition of retro-illumination and/or contrast data sets. This limitation did not allow compensation for some of the individual and environmental factors that might occur between data acquisitions, such as humidity, tear quality, lighting, and airflow. Although these factors might affect variability within subject data, they would not be expected to impact the overall outcome of this study.

The illumination used for testing may have been a factor. The RVC and retro-illumination data was acquired with standard biomicroscope illumination, while the CS

was not. The typical biomicroscope illumination contains IR spectrum created by an incandescent bulb. The Zeiss 20 SL biomicroscope used in this study contained a built-in IR filter reducing some of the IR spectrum. Although, we found additional reduction possible with the accessory "red-free" or "cobalt blue" filters (figure 18), standard illumination was used for this study. The inclusion of IR wavelengths may have impacted tear film stability. The result of IR inclusion would be expected to affect the onset and/or the amount of contrast decrement, but not the process nor the trend of tear film disruption.

CONCLUSIONS

The techniques describe in this study can be used to quantify the effects of tear film breakup objectively, in real time. The effect of tear film disruption is profound and produces dramatic effects on vision. Tear film disruption results in a drastic reduction of optical performance of the eye, leading to reduced contrast sensitivity and degraded optical images. Tear film disruption occurs under many ocular conditions such as dry eye disorders and contact lens wear. Environmental factors such as pollution, humidity and airflow also play a role in tear film stability [8, 27, 35, 71, 72]. These data support the hypothesis that an intact and regular tear film provides an essential optical surface for the eye.

17

BIBLIOGRAPHY

1.   Moses R. The Cornea. In: Moses R, ed. Adler's Physiology of the Eye, St. Louis, Toronto, London: The C.V. Mosby Company, 1981:38-61.

2.   Newell W. Ophthalmology, Principles and Concepts. In: ed. C.V. Mosby, 1982:73-4.

3.   Mandell R. Contact Lens Practice. 4th ed, Springfield. IL: Charles Thomas, 1988.

4.   Borish I, Greenberger M, Heath G, Ludlam W, Rosenbloom A, Sarver M, Wild B. The Refractive Status of the Eye - Components and Correlation. In: Borish I, ed. Clinical Refraction, vol 1. Chicago, IL: The Professional Press, 1975:47-81.

5.   Bartlett J, Jannus S. Clinical Ocular Pharmacology. Boston, London, Syndey ,Wellington ,Durban ,Toronto: Butterworth Publishers, 1984.

6.   Holly F. Formation and Stability of the Tear Film. In: Holly F, Kemp M, ed. The Preocular Tear Film and Dry Eye Syndromes (International Ophthalmology Clinics), vol 13. Boston: Little Brown, 1973:73.

7.   Holly F. Tear Film Formation and Rupture: An Update. In: Holly FJ, ed. The Preocular Tear Film In Health, Disease, and Contact Lens Wear, Lubbock TX: Dry Eye Institute, Inc, 1986:634-45.

8.   Schwartz CA. Specialty Contact lenses: A Fitter's Guide. 1st ed, Philadelphia, London, Toronto, Montreal, Sydney, Tokyo: WB Saunders Company, 1996.

9.   Rieger G. The Importance of Precorneal Tear Film for the Quality of Optical Imaging. Br-J-Ophthamol 1991;76:157-8.

10.   Katzung B. Basic & Clinical Pharmacology. 6th ed, Norwalk, Connecticut: Appleton & Lange, 1995.

11.   Cline D, Hofstetter H, Griffin J. Dictionary of Visual Science. Radnor, Pennsylvannia: Chilton Book Company, 1980.

12.   Timberlake G, Doane M, Bertera J. Short-Term, Low Contrast Visual Acuity Reduction Associated with in Vivo Contact Lens Drying. OPTOMETRY AND VISION SCIENCE 1992;69:755-60.

13.   Vaughan D, Asbury T. Tears. In: ed. General Ophthalmology, Lange Medical Publications, 1983:52-7.

14.   Young G, Elfron N. Characteristics of the pre-lens tear film during hydrogel contact lens wear. Ophthal Physiol Opt 1991;11:53-8.

15.   Fatt I. Observations of Tear Film Break up on Model Eyes. CLAO 1991;17:267-81.

16.   Brown B, Cho P, Yap M. Mechanical manipulation of the lids and tear break-up time measurements in Hong Kong Chinese. Ophthal Physiol Opt 1993;1993:233-8.

17.   Bussacker H. Tear Analysis and Its Significance in Contact Lens Fitting. Contact Lens Spectrum 1997;35-40.

18.   Cho P, Brown B, Chan I, Conway R, Yap M. Reliability of the Tear Break-up Time Technique of Assessing Tear Stability and the Locations of the Tear Break-up in Hong Kong Chinese. Optometry and Vision Science 1992;69:879-85.

19.   Cho P, Douthwaite W. The Relation between Invasive and Noninvasive Tear Break-up Time. Optometry and Vision Science 1995;72:17-22.

20.   Cho P, Yap M. Age, Gender, and Tear Break-up Time. Optometry and Vision Science 1993;70:828-31.

21.   Cho P, Brown B. Review of the Tear Break-up Time and a Closer Look at the tear Break-up Time on Hong Kong Chinese. Optometry and Vision Science 1992;70:30-8.

22.   Holly F. Diagnostic Methods on Treatment Modalities of Dry Eye Conditions. International Ophthalmology 1993;17:113-25.

23.   Korb D. Tear Film - Contact Lens Interactions. In: Sullivan DA, ed. Lacrimal Gland, Tear Film, and Dry Eye Syndromes, New York: Plenum Press, 1994:403-10.

24.   Korb D, Baron D, Herman J, Finnemore V, Exford J, Hermosa J, Leahy C, Glonek T, Greiner J. Tear Film Lipid Layer Thickness as a Function of Blinking. Cornea 1994;13:354-9.

25.   Lemp M. Report of the National Eye Institute/Industry Workshop on Clinical Trials in Dry Eyes. CLAO 1995;21:221-32.

26.   Toda I, Fujishima H, Tsubota K. Ocular Fatigue is the Major Symptom of Dry Eye. ACTA Ophthalmologica 1993;71:347-52.

27.   Toda I, Shimazaki J, Tsubota K. Dry Eye with Only Decreased Tear Break-up Time is Sometimes Associated with Allergic Conjunctivitis. Ophthalmology 1994;102:302-9.

28.   Yokoi N, Takehisa Y, Kinoshita S. Correlation of Tear Lipid Layer Interference Patterns with the Diagnosis and Severity of Dry Eye. American Journal of Ophthalmology 1996;122:818-24.

29.   Patel S, Farrell J, Bevan R. Relation between Precorneal Tear Film Stability and Tear Production Rate in Normal Eyes. Optometry and Vision Science 1989;66:300-3.

30.   Beebe W, Esquivel E, Holly F. Comparison of Lacrimation Kinetics in Dry Eye Patients and Normals. Current Eye Research 1988;7:419-25.

31.   Bjerrum K. Test and Symptoms in Keratoconjunctivitis Sicca and their Correlation. ACTA Ophthalmol Scand 1996;74:436-41.

32.   Lavaux J, Keller W. Lacrimal Equilibration Time (LET): A Quick and Simple Dry Eye Test. Optometry and Vision Science 1993;70:832-8.

33.   Lin S, Brenner H. Stability of the Tear Film. In: Holly FJ, ed. The Preocular Tear Film In Health, Disease, and Contact Lens Wear, Lubbock TX: Dry Eye Institute, Inc, 1986:670-6.

34.   Norn M. Tear Film Break-Up Time. A Review. In: Holly FJ, ed. The Preocular Tear Film In Health, Disease, and Contact Lens Wear, Lubbock TX: Dry Eye Institute, Inc, 1986:52-6.

35.   Norn M. Pollution Keratoconjunctivitis, A Review. ACTA Ophthalmologica 1992;70:269-73.

36.   Sheedy J. The Bottom Line on Fixing Computer Related Vision and Eye Problems. J Am Optom Assoc 1996;67:512-7.

21

37.   Tsubota K, Nakamori K. Effects of Ocular Surface Area and Blink Rate on Tear Dynamics. Arch Ophthalmology 1995;113:155-8.

38.   Yap M. Tear Break-up is related to Blink Frequency. ACTA Ophthalmologica 1991;69:92-4.

39.   Lohmann C, Fitske F, O'Brart D, Muir M, TImberlake G, Marshall J. Corneal Light Scattering and Visual Performance in Myopic Individuals with Spectacles, Contact Lenses, or Excimer Laser Photorefractive Keratectomy. Am J Ophthalmol 1993;115:444-53.

40.   Dilly P. Structure and Function of the Tear Film. In: Sullivan DA, ed. Lacrimal Gland, Tear Film, and Dry Eye Syndromes, New York: Plenum Press, 1994:239-47.

41.   Tiffany J. Composition and Biophysical Properties of the Tear Film: Knowledge and Uncertainty. In: Sullivan DA, ed. Lacrimal Gland, Tear Film, and Dry Eye Syndromes, New York: Plenum Press, 1994:231-8.

42.   Milder B. The Lacrimal Apparatus. In: Moses R, ed. Adler's Physiology of the Eye, St. Louis, Toronto, London: The C.V. Mosby Company, 1983:16-37.

43.   Prydal J, Kerr Muir M, Dilly P. Comparison of tear film thickness in three species determined by the glass fibre method and confocal microscopy. Eye 1993;7:472-5.

44.   Prydal J, Campbell F. Study of precorneal tear film thickness and structure by interferometry and confocal microscopy. Invest Ophthalmo Vis Sci 1992;33:1996-2005.

45.   Prydal J, Artal P, Woon H, Campbell F. Study of Human Precorneal Tear Thickness and Structure by Interferometry. Invest Ophthalmo Vis Sci 1992;33:2006-11.

46.   Cronje-Dunn S, Harris WF. Keratometric variation: the influence of a fluid layer.
Ophthalmology and Physiological Optics 1996;16:234-6.

47.   Padday J. Cohesive properties of thin films of liquids adhering to a solid surface.
Spec Disc Faraday Soc 1970;64:

48.   Benjamin W, Borish I. Physiology of aging and its influence on the contact lens
prescription. Journal of the American Optometric Association 1991;62:743-53.

49.   Little S, Bruce A. Role of the Post-Lens Tear Film in the Mechanism of Inferior
Arcuate Staining with Ultrathin Hydrogel Lenses. CLAO 1995;21:175-81.

50.   Westheimer G, Liang J. Influence of Ocular Light Scatter on the Eye's Optical
Performance. Optical Society of America 1995;12:1417-24.

51.   Mathers W, lane J, Sutphin J, Zimmerman MB. Model for Ocular Tear Film
Function. Cornea 1996;15:110-9.

52.   Miller D, Nadler MP. Light Scattering: Its Relationship to Glare and Contrast in
Patients and Normal Subjects. In: ed.

53.   Paulsson L-E, Sjostrand. Contrast Sensitivity in the presence of a glare light.
Assoc for Res in Vis and Ophthal 1980;401-6.

54.   Thaung J, Beckman C, Abrahamsson M, Sjostrand J. The Light Scattering Factor.
Investigative Ophthalmology and Visual Science 1995;36:2313-7.

55.   Adamsons I, Rubin G, Vitale S, Taylor H, Stark W. The Effects of Early
Cataracts on Glare and Contrast Sensitivity: A Pilot Study. Arch Ophthalmology
1992;110:1081-6.

56.   Finlay D, Wilkinson J. The Effects of Glare on the Contrast Sensitivity Function. The Human Factors Society 1984;26:283-7.

57.   Westheimer G. The Oscilloscopic View: Retinal Illumination and Contrast of Point and Line Targets. Vision Res 1985;25:1097-103.

58.   de Waard P, IJspeert J, van den Berg T, de Jong P. Intraocular Light Scattering in Age-Related Cataracts. Investigative Ophthalmology and Vision Research 1992;33:618-25.

59.   Wolfe JM. An Introduction to Contrast Sensitivity Testing. In: ed. Glare and Contrast Sensitivity for Clinicians, 1990:5-23.

60.   Hess R, Woo G. Vision through Cataracts. Association for Research in Vision and Ophthalmology 1978;0146-020/78/0517-0428:428-35.

61.   Albarran C, Pons AM, Lorente A, Montes R, Artigas JM. Influence of the Tear Film on Optical Quality of the Eye. Contact Lens and Anterior Eye 1997;20:129-35.

62.   Manivannan A, Sharp P, Phillips R, Forrester V. Digital Fundus Imaging using a Scanning Laser Ophthalmoscope. Physiological-Measurement 1993;14:43-56.

63.   Gilchrist J. Computer Processing of Ocular Photographs - A Review. Ophthal Physio Opt 1987;7:379-80.

64.   Goldbaum M, Katz N, Nelson M, Haff L. The Discrimination of Similarly Colored Objects in Computer Images of the Ocular Fundus. Investigative Ophthalmology and Visual Science 1990;31:617-23.

65.   Varma R, Spaeth G. The PAR IS 2000: a new System for Retinal Digital Image Analysis. Ophthalmic Surgery 1988;19:183-92.

24

66.   Bradley A, Hook J, Haeseker J. A Comparison of Clinical Acuity and Contrast Sensitivity Charts: Effect of Uncorrected Myopia. Ophthalmology and Physiological Optics 1991;11:218-26.

67.   Johnson C, Casson E. Effects of Luminance, Contrast, and Blur on Visual Acuity. Optometry and Vision Science 1995;72:864-9.

68.   Legge GE, Mullen KT, Woo GC, Campbell FW. Tolerance to Visual Defocus. Optical Society of America 1987;4:851-63.

69.   Thorn F, Schwartz F. Effects of Dioptric Blur on Snellen and Grating Acuity. Optometry and Vision Science 1990;67:3-7.

70.   Zhang Y, Bradley A, Thibos L. Apodization" by the SCE moderates the visual impact of retinal image defocus. submitted to JOSA A 1998;

71.   Franck C, Bach E, Skov P. Prevalence of Objective Eye manifestations in people working in Office Buildings with Different Prevalences of the Sick Building Syndrome Compared with the General Population. Int Arch Occup Environ Health 1993;65:65-9.

72.   Korb D, Greiner J, Glonek T, Esbah R, Finnemore V, Whalen A. Effect of Periocular Humidity on the Tear Film Lipid Layer. Cornea 1996;15:129-34.
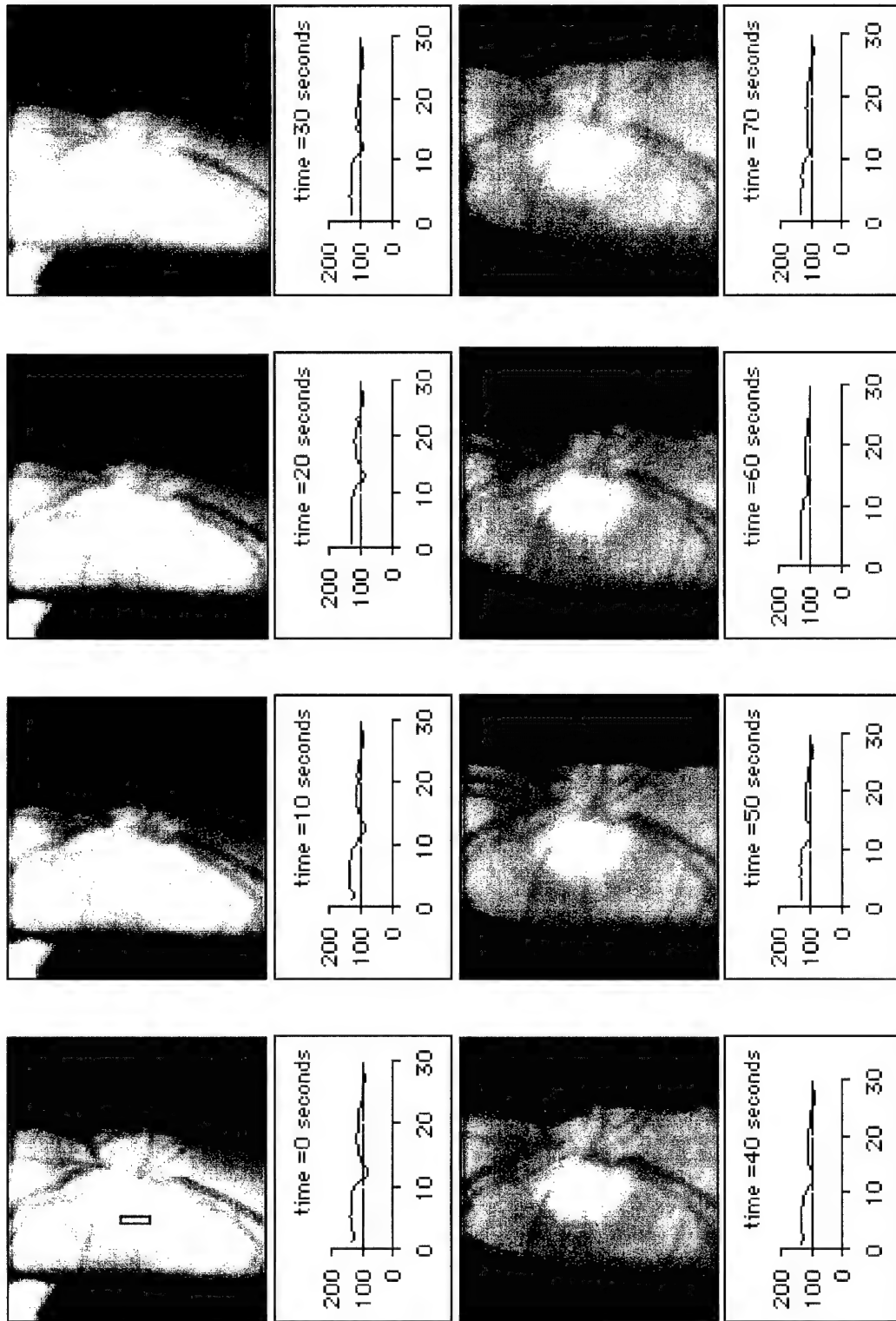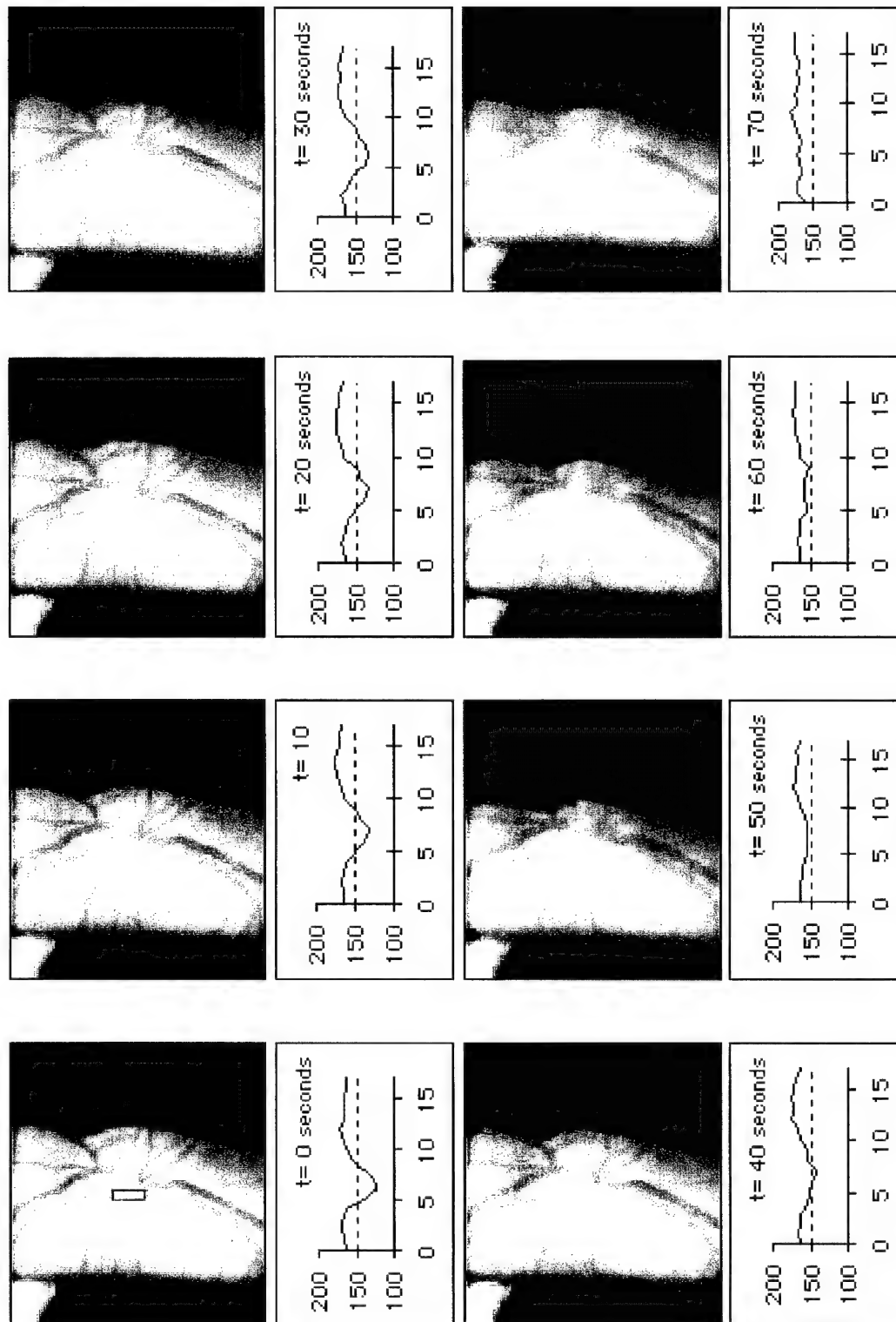
Figure 1
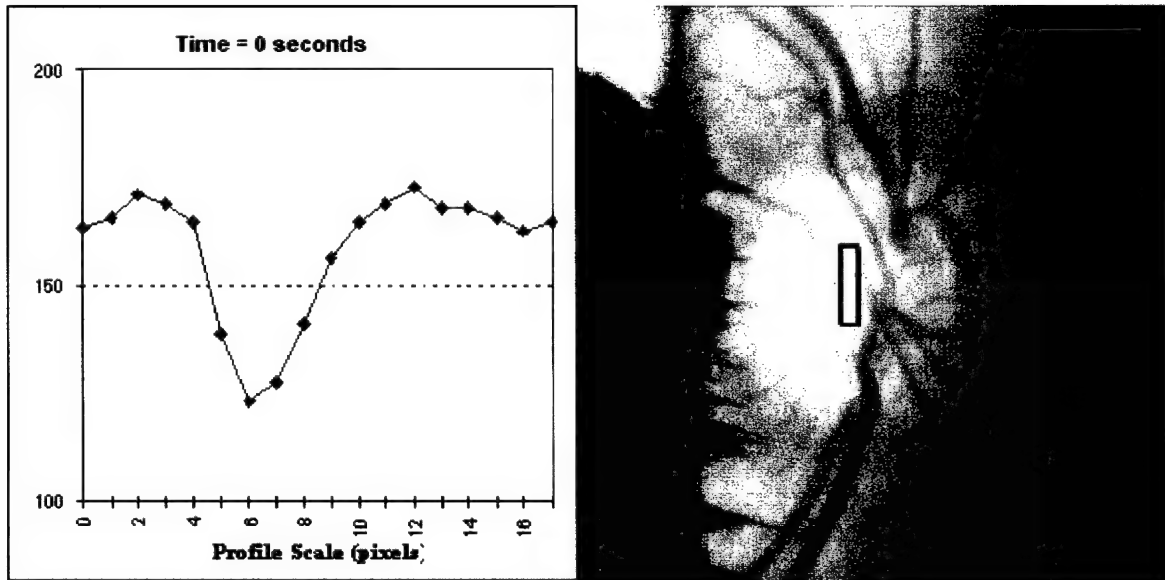
NIH-image program (NIH-Image version 1.60, (http://rsb.info.nih.gov/nih-image/) was used to create a region of interest (ROI) and to generate an intensity profile for each sequential profile. An example of a ROI is displayed above, outlined here in red. The dimensions of the ROIs used in this study were 5 pixels in width and approximately 50 pixels in length. The length of the ROI was varied to enhance vessel and background recognition.. Pixel data across the width was averaged and the averaged data create an intensity profile (see graph above). The same ROI was used for each image in a series. The vessel intensity (the intensity profile "valley") and an adjacent background intensity (the average of the "peak" on either side of the vessel) are determined for each serial image. Weber's definition of contrast "(delta L)/L" was applied to determine retinal vessel contrast.
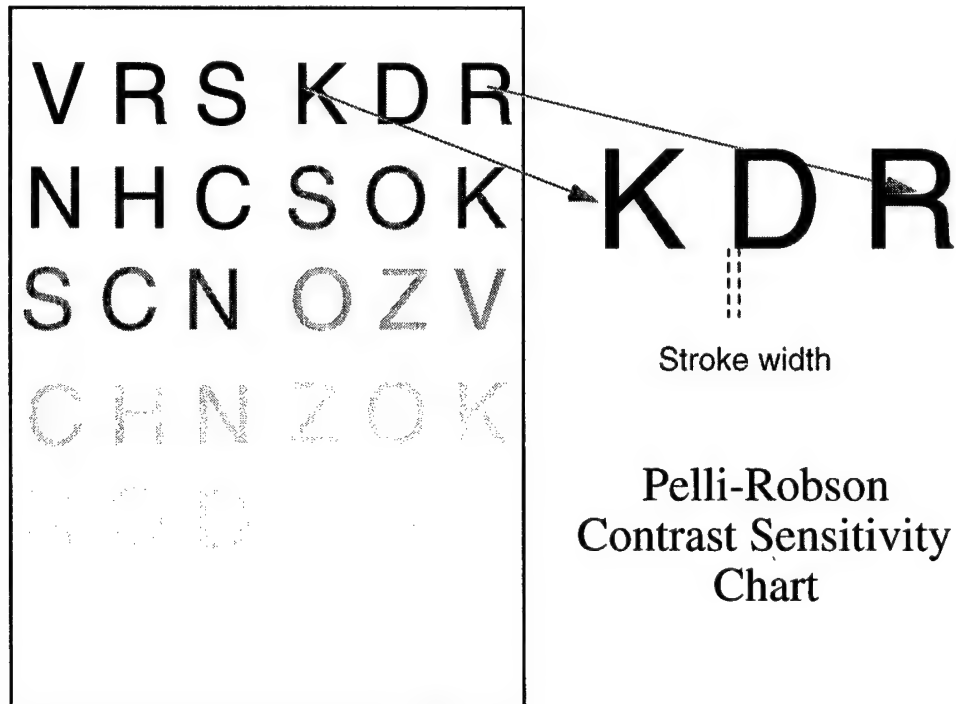
Figure 2

Images and Profiles from "Without SCL" retinal vessel data

Figure 3

Images and Profiles from "With SCL" retinal vessel data

28

Figure 4

Stroke width

Pelli-Robson
Contrast Sensitivity
Chart

A Pelli-Robson contrast sensitivity chart (simulated above) was positioned two meters from the subject. At this distance the stroke width of the chart font was approximately equal to the angular size of the video recorded retinal vessels (approximately 17-18 arc minutes). The subject viewed the chart prior to each test cycle. The minimum recognizable letter group (recognizing 3 of 3 letters) was determined and recorded. The test cycle began as the subject fixated on this initial letter group and suspended blinking as long as possible. During the non-blinking test period, the subject reported loss of the minimum letter group recognition and then immediately refixated on next recognizable group. This process continued until the subject initiated a blink. The series of minimum recognizable letter group and elapsed time to recognition loss were recorded and later analyzed.

Figure 5
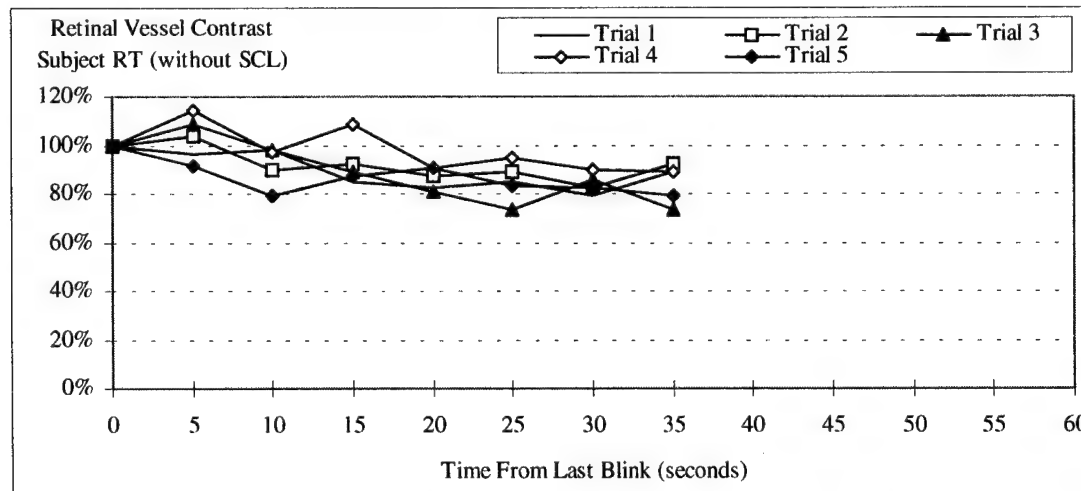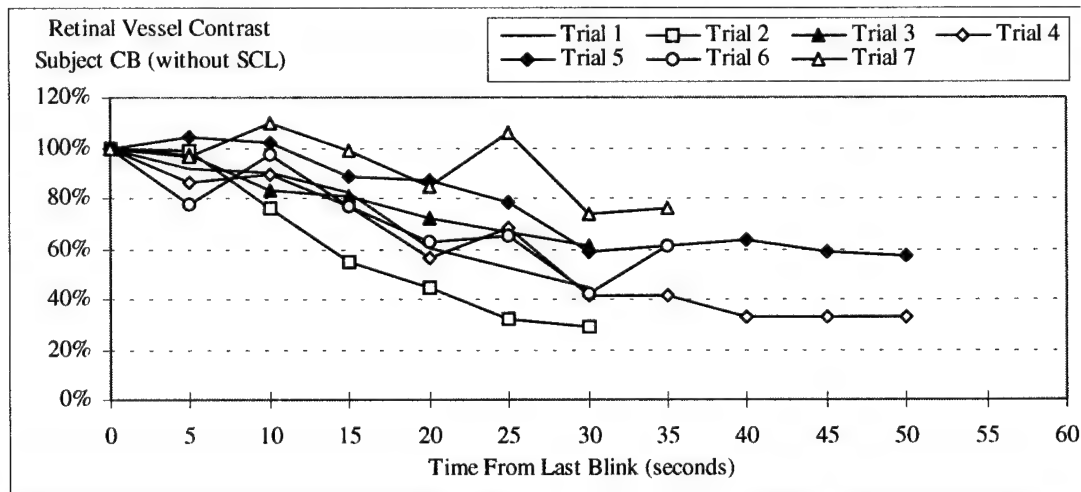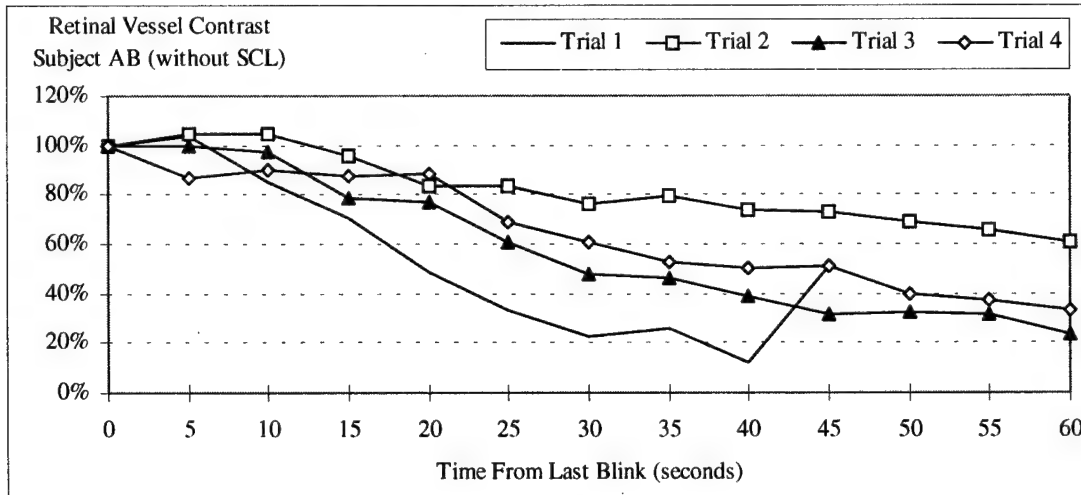
"WITHOUT SCL" Retinal Vessel Contrast: Individual data

Figure 6
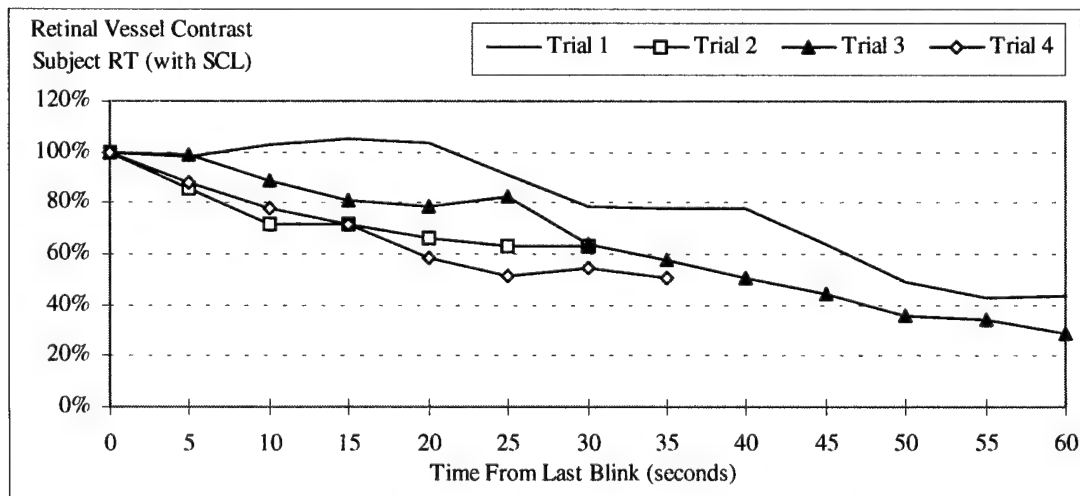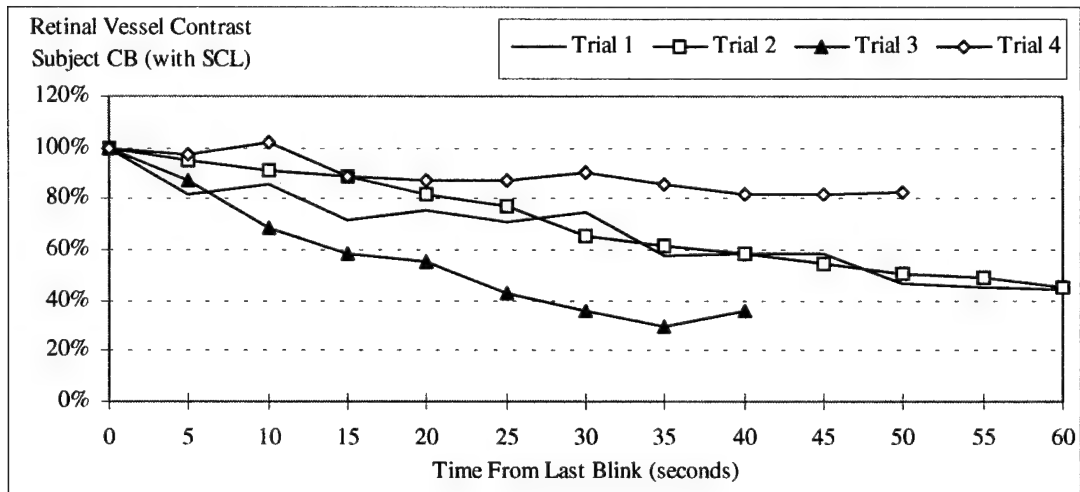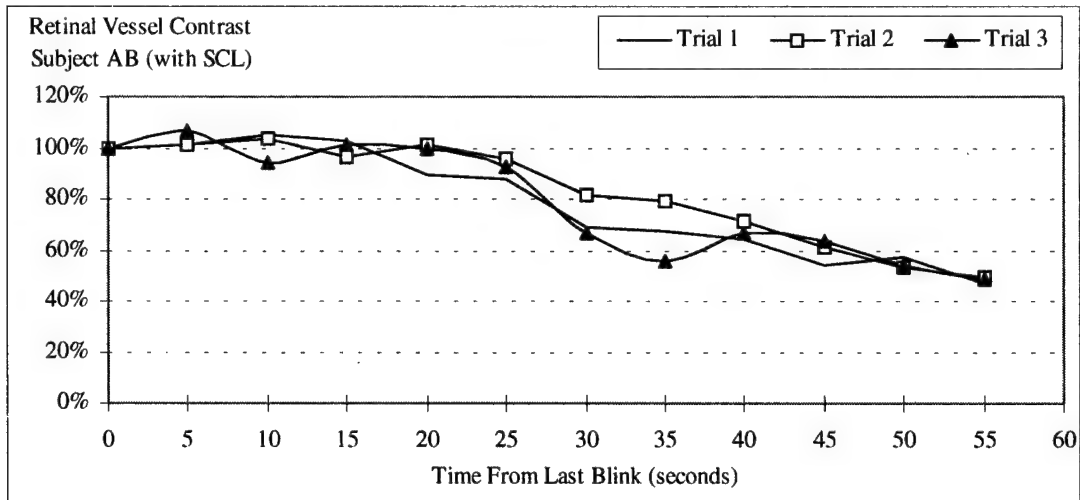
"WITH SCL" Retinal Vessel Contrast: Individual data

Figure 7
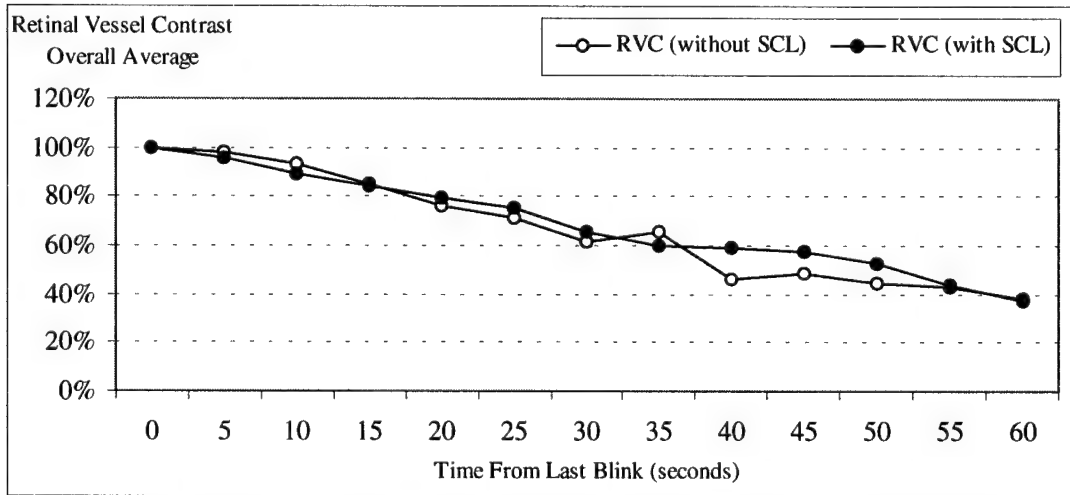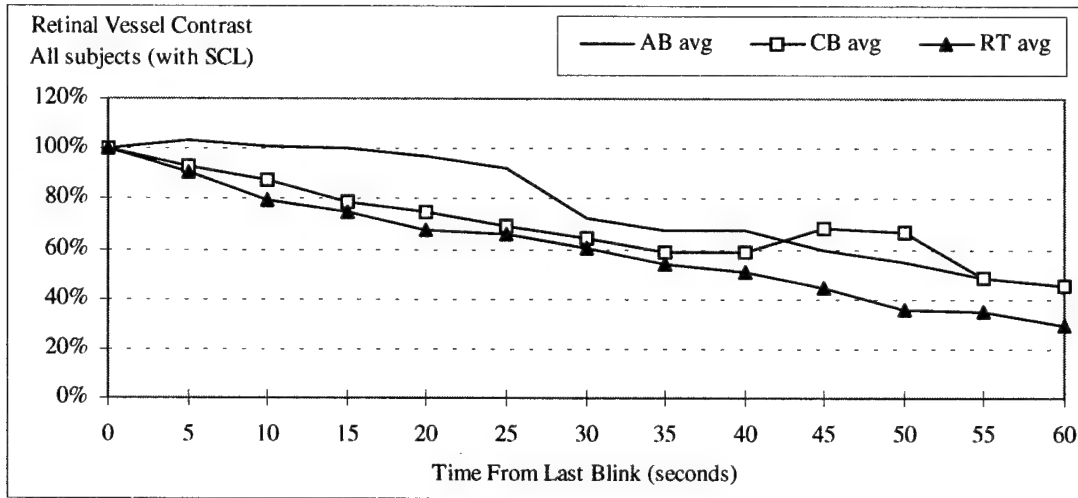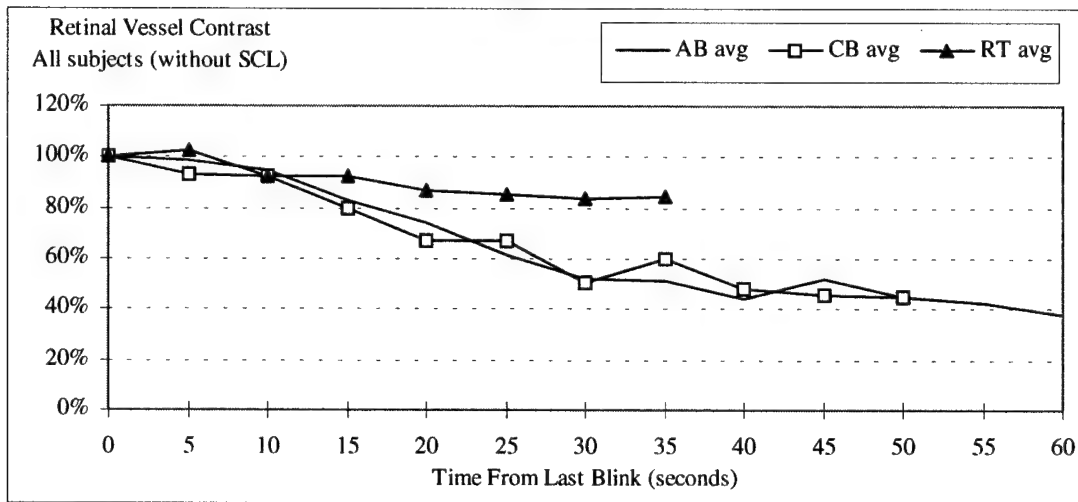
"WITHOUT and WITH SCL" Retinal Vessel Contrast: Averaged data

Figure 8
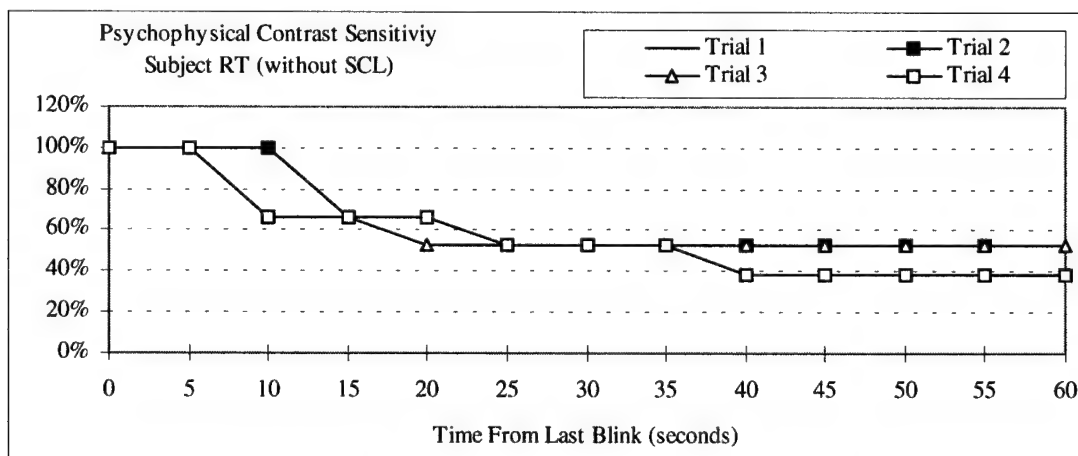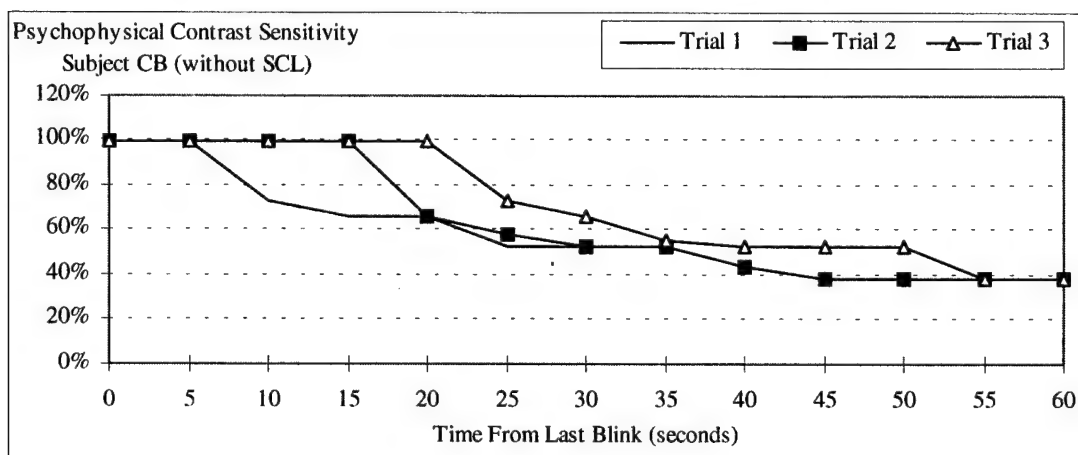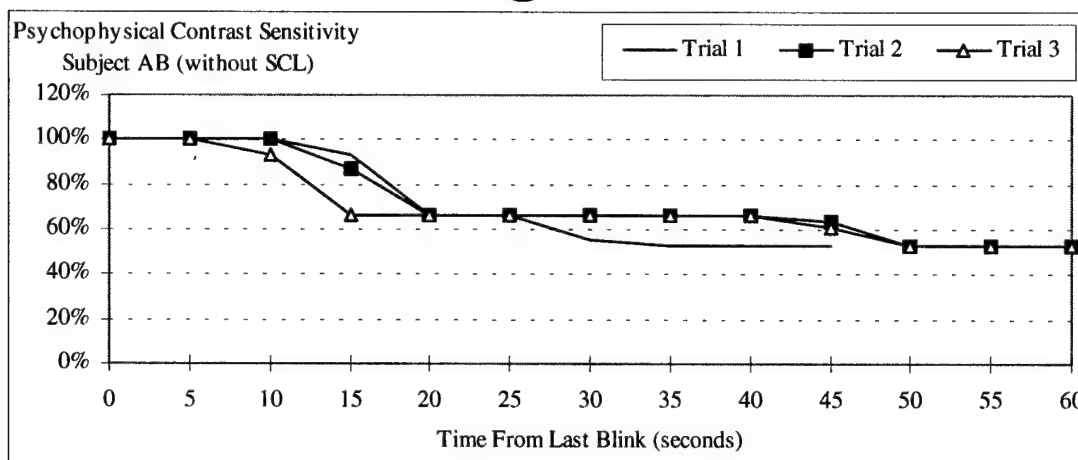
"WITHOUT SCL" Contrast Sensitivity: Individual data

Figure 9
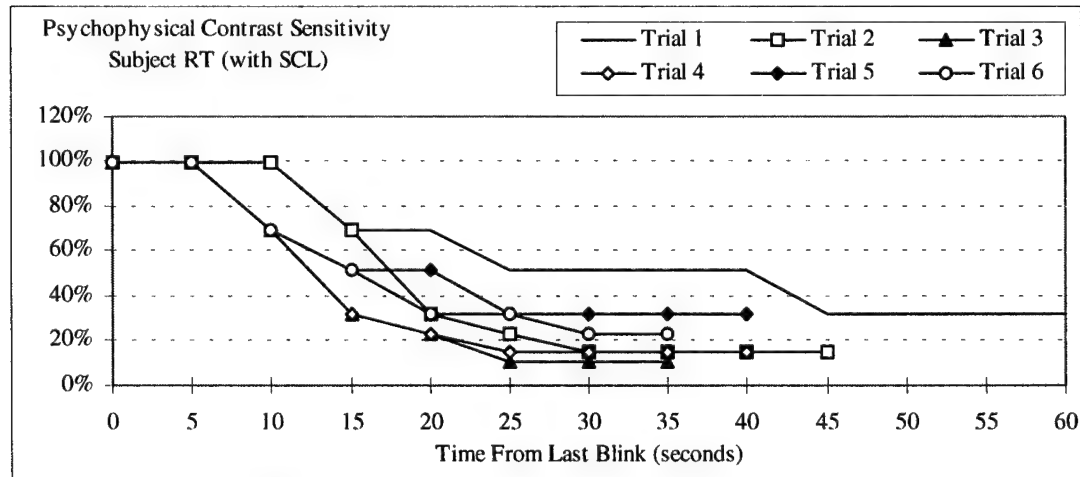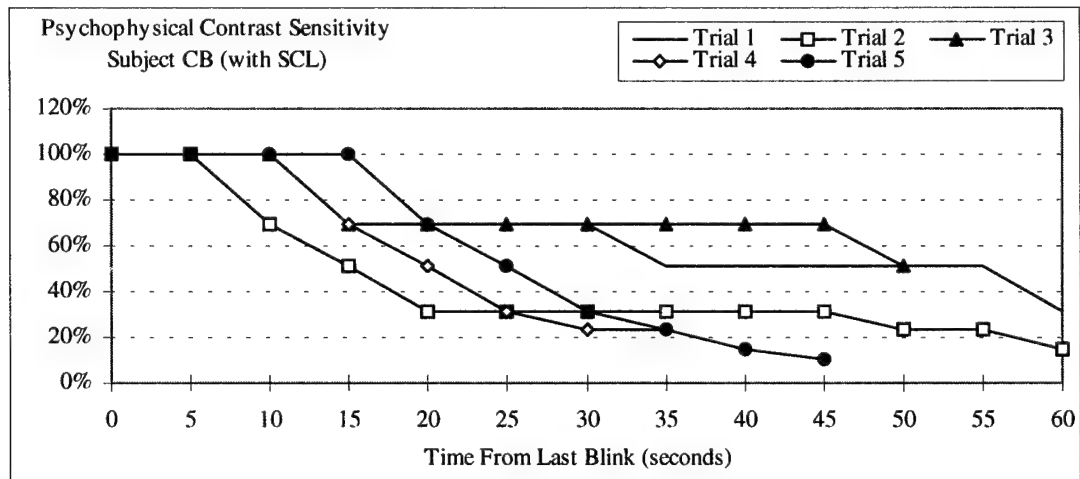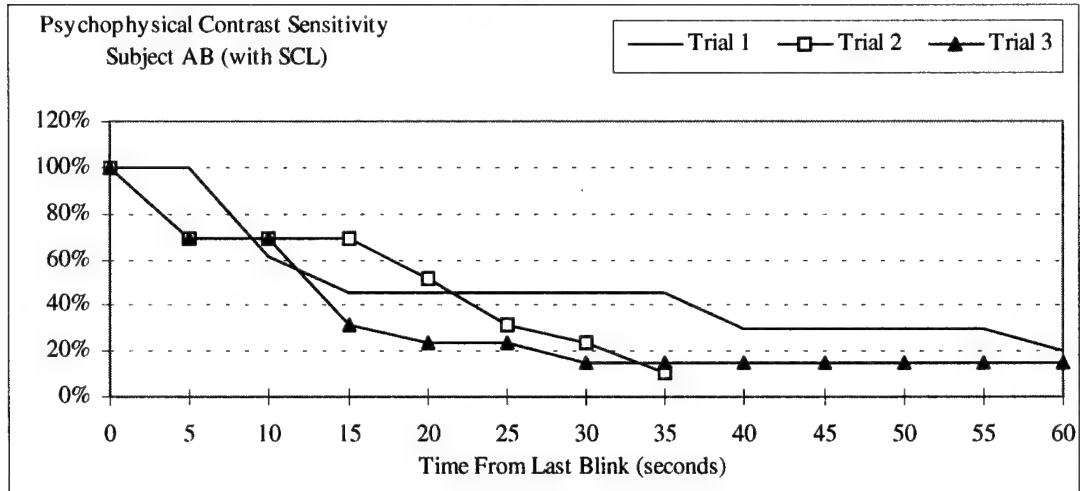
"WITH SCL" Contrast Sensitivity: Individual data

Figure 10
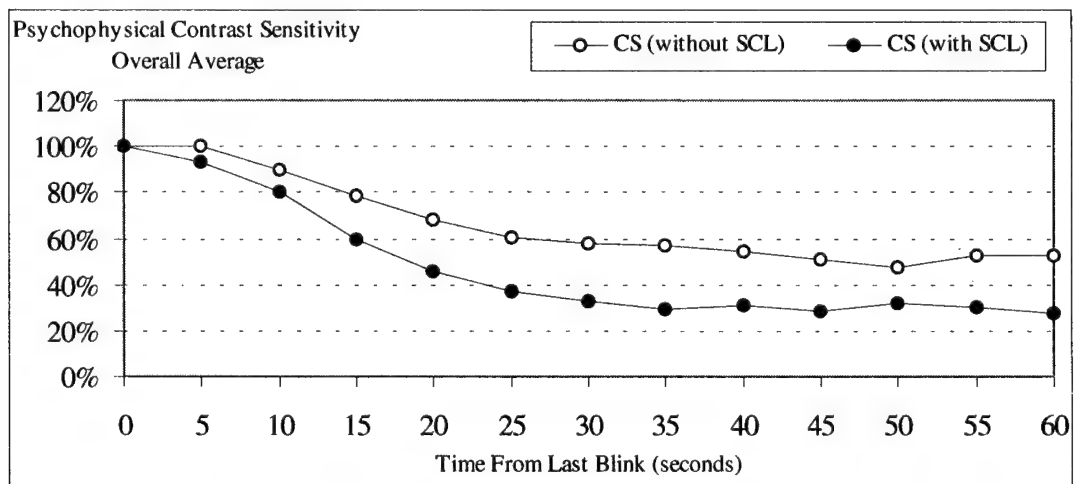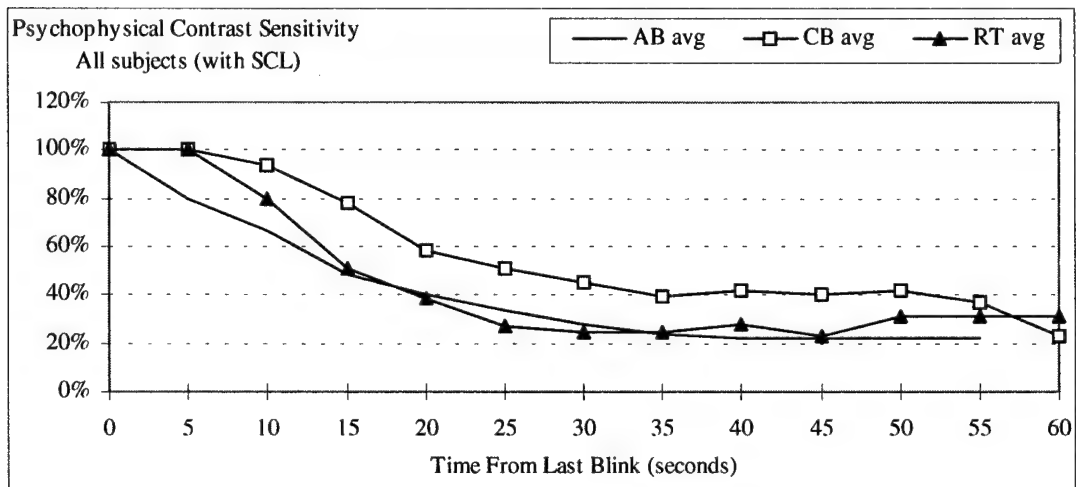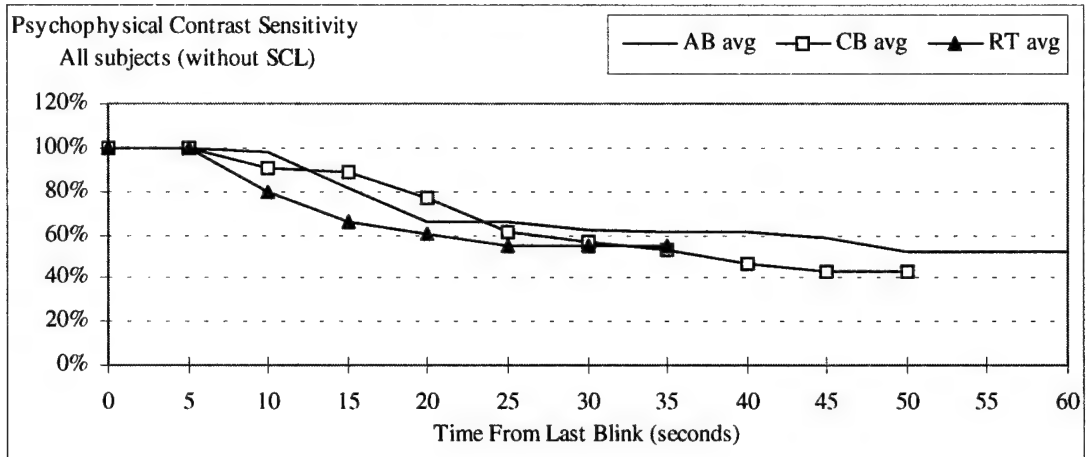
"WITHOUT and WITH SCL" Contrast Sensitivity: Averaged data

35
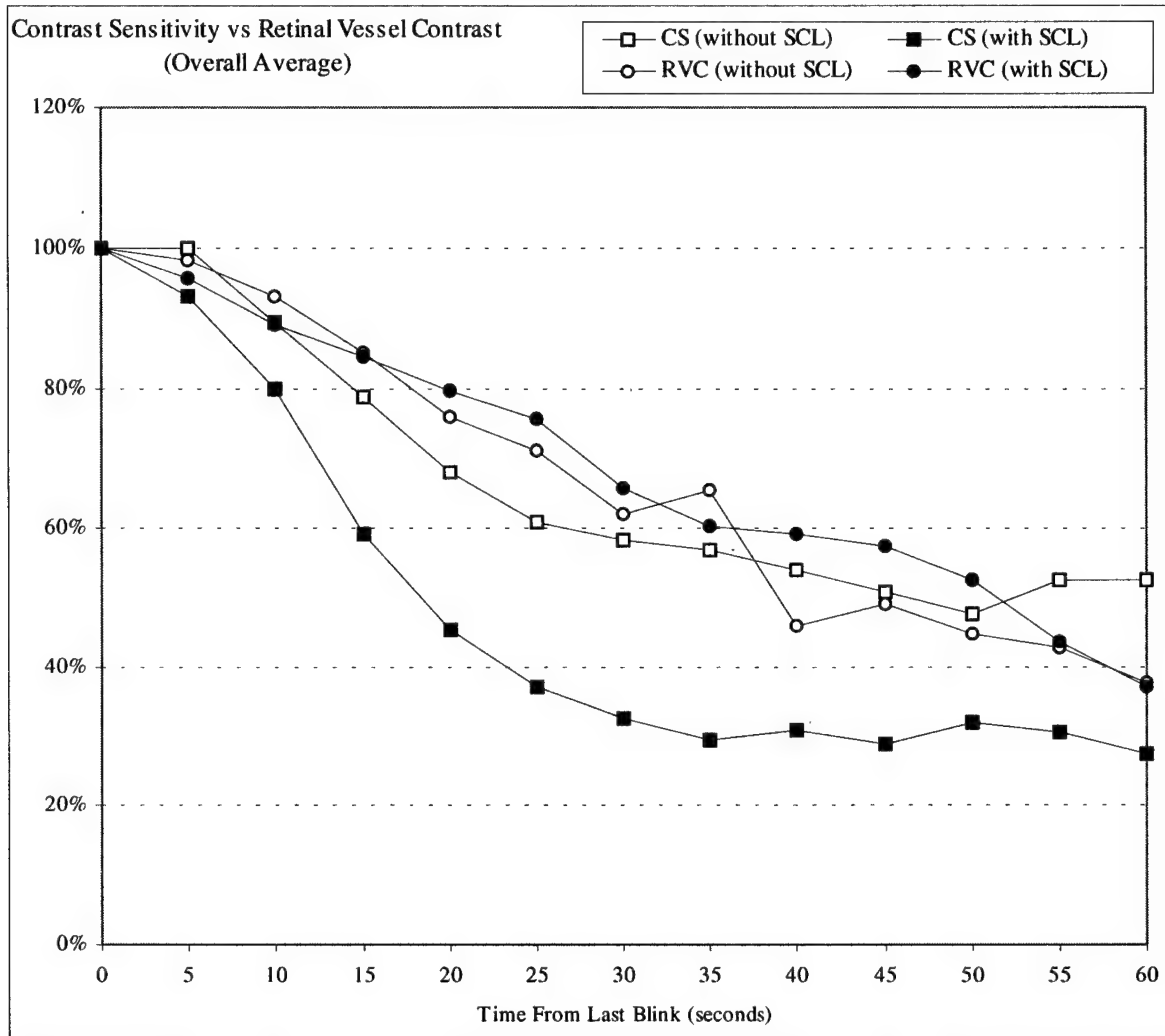
Figure 11

"WITHOUT and WITH SCL" Retinal Vessel Contrast / Contrast Sensitivity
Averaged data

Figure 12

15 seconds   10 seconds   5 seconds   0 seconds

35 seconds   30 seconds   25 seconds   20 seconds
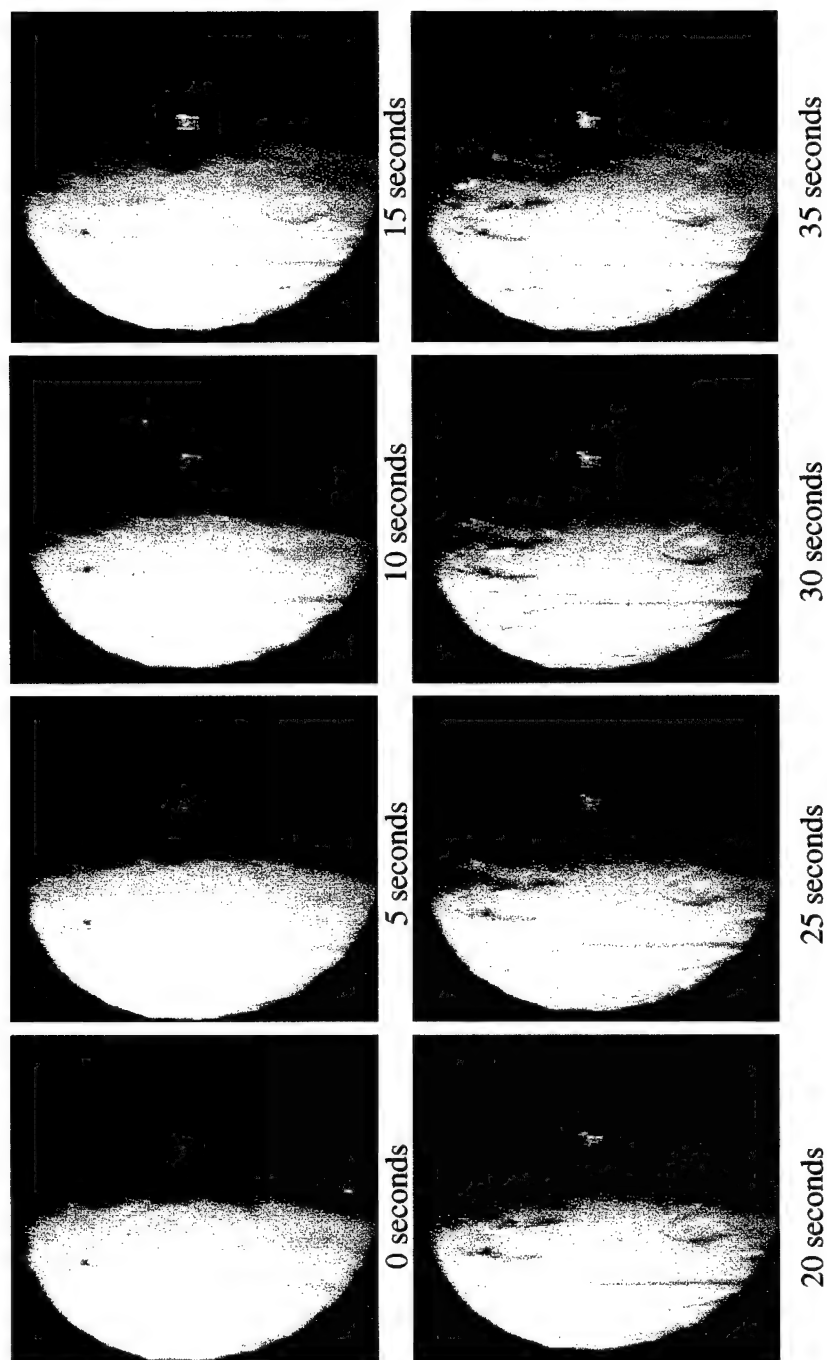
Retro-illumination, Without SCL

Figure 13

15 seconds

35 seconds

10 seconds

30 seconds

5 seconds

25 seconds

0 seconds

20 seconds

Retro-illumination, Without SCL

38

Figure 14

0 seconds   5 seconds   10 seconds   15 seconds

20 seconds   25 seconds   30 seconds   35 seconds
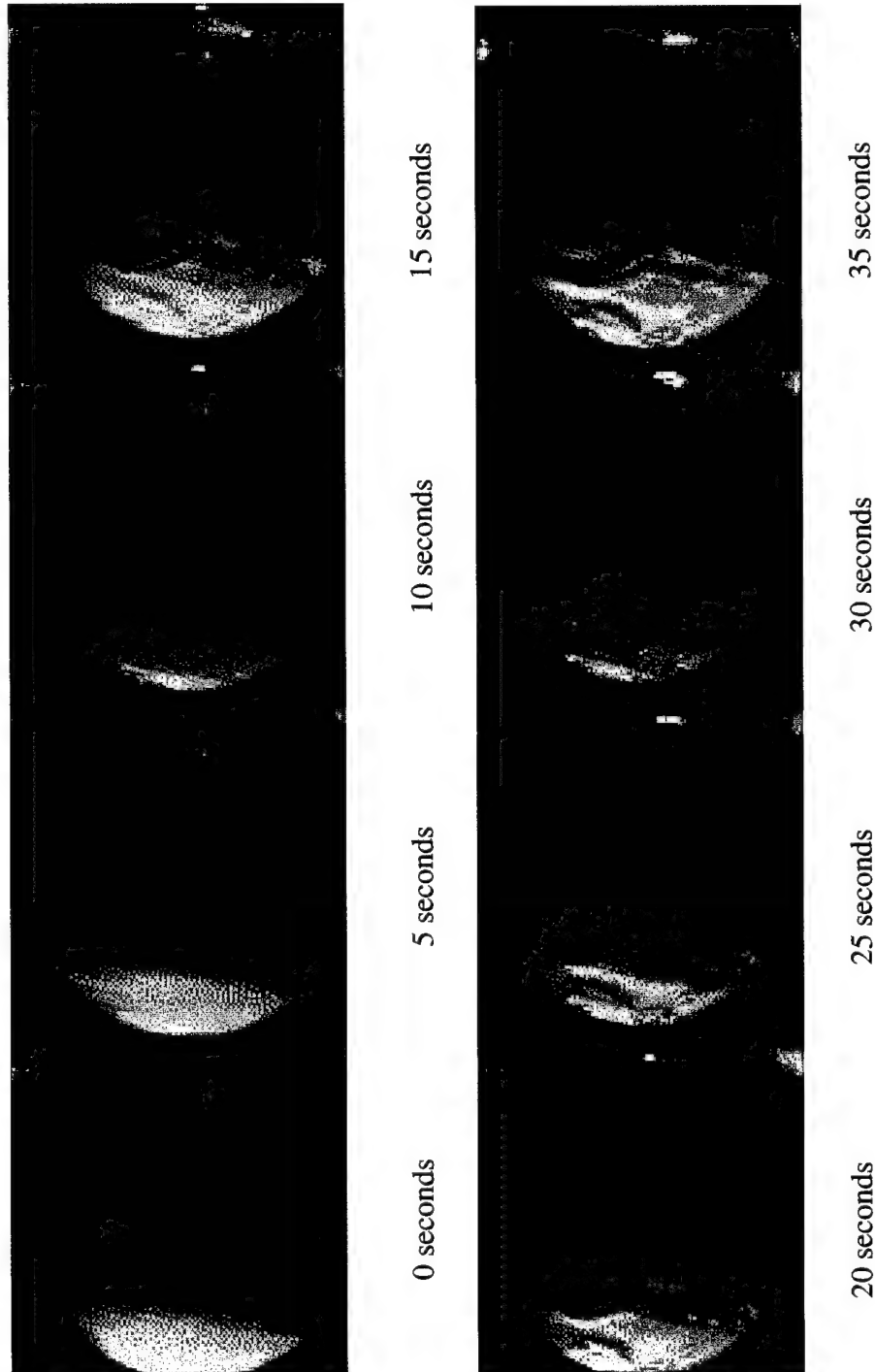
Retro-illumination, With SCL

Figure 15

15 seconds

35 seconds

10 seconds

30 seconds

5 seconds

25 seconds

0 seconds

20 seconds

Retro-illumination, With SCL

40

Figure 16

Effect of Defocus on Contrast Sensitivity ——— Normal CSF - - - - Defocused CSF

Contrast Sensitivity

Frequency (Cycle/Degree)
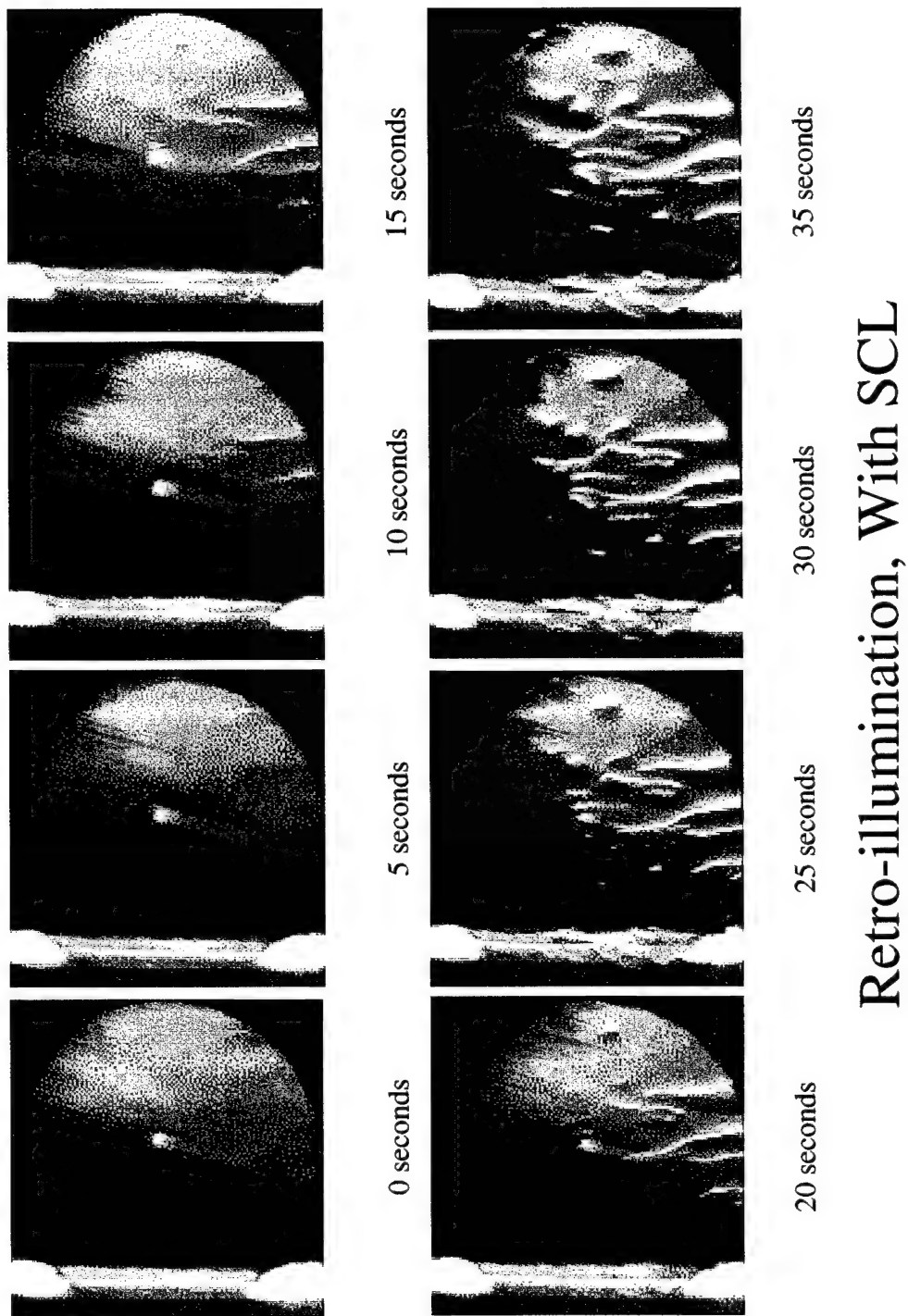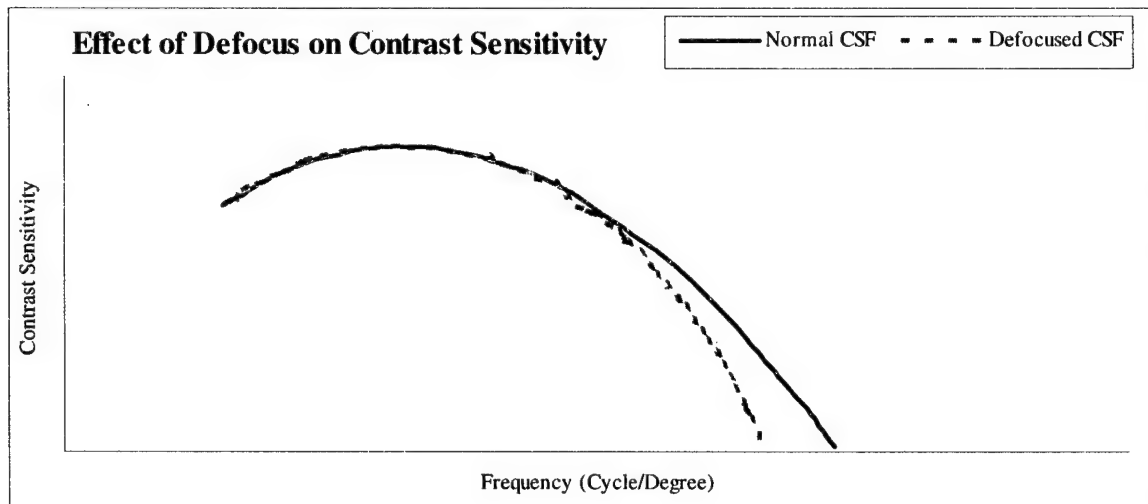
The effect of optical defocus on contrast sensitivity functions: Contrast Sensitivity at higher spatial frequencies is reduced by small to moderate amounts of defocus. Contrast sensitivity at lower spatial frequencies is relatively insensitive to small and moderate amounts of defocus.

Figure 17

Effect of Scatter on Contrast Sensitivity ——— Normal CSF - - - - CSF with Scatter

Contrast Sensitivity

Frequency (Cycle/Degree)
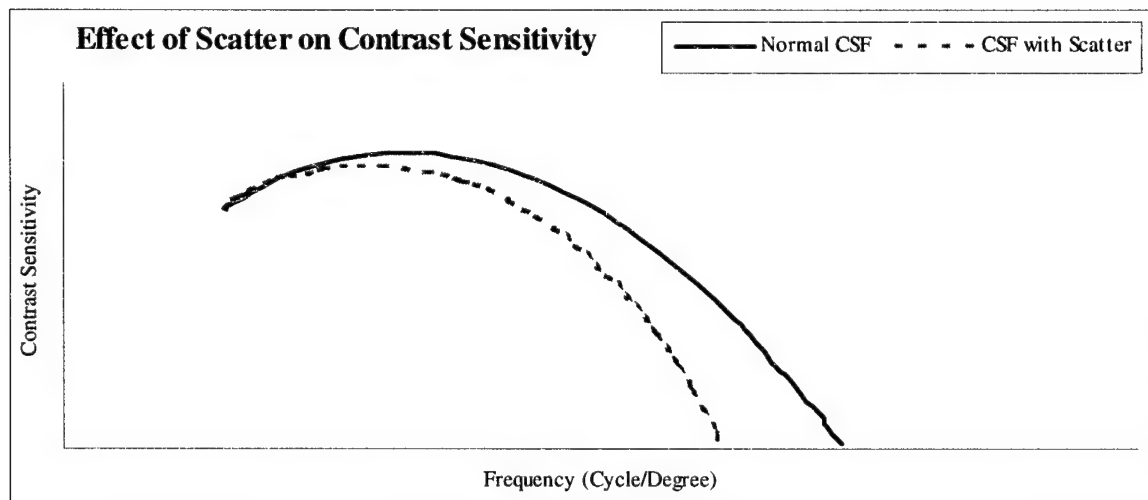
The effect of optical scatter on contrast sensitivity functions: Contrast sensitivity at lower spatial frequencies is relatively less sensitive to reduction due to scatter. However, with increasing amounts of scatter, all spatial frequencies are reduced by scatter.

Figure 18
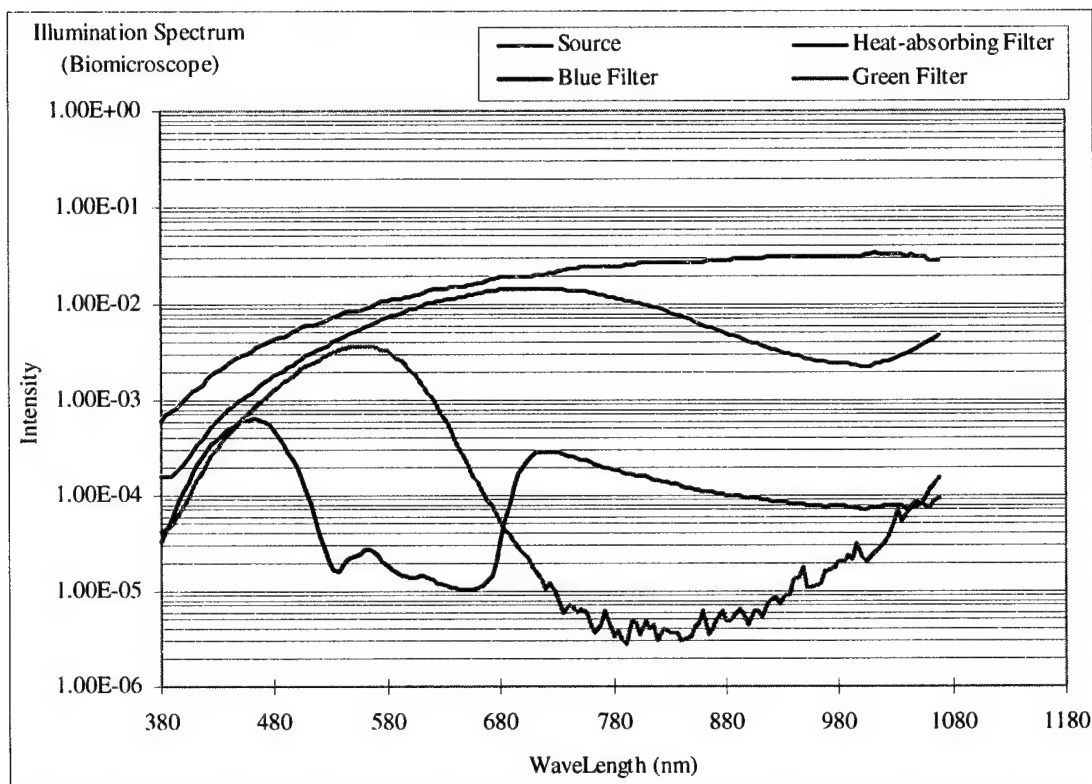
Illumination spectrum from standard biomicroscope (Zeiss Slit Lamp: 20 SL). The light source is a 6 Volt, 20 Watt halogen lamp. Product literature describes three filters available on this slit lamp; a "swing-in blue" (cobalt) filter, a "swing-in green" (red free) filter, and a permanently integrated "heat-absorbing" (infra-red) filter. The spectrum data displayed above was obtained using a spectrometer. The source illumination measurement was obtained by direct measure of the halogen lamp. The other illumination measurements (heat-absorbing, blue, and green) were obtained from an indirect measure using a white diffuser positioned at the subject plane.

Dry Eye - Diagnostic Methods [1,2,3,4]

Clinical Presentation:

- Subjectively persistent ocular discomfort

  - sandy, gritty feeling that may wax and wane with time

  - foreign body sensation without visible culprit

  - burning sensation

  - red, irritated eyes

  - excessive tearing

  - ocular discomfort upon wakening or in late afternoon

  - excessive mucus discharge

  - photophobia

  - Sensitive to drafts (air flow)

  - vision disturbances during extended reading, computer monitor or television viewing

  - ocular fatigue [5]

- Slit Lamp (biomicroscope) findings

  - debris in the tear film

  - the presence of threads of filaments

  - uneven, diminished tear meniscus (with or without fluorescein)

Tear Related:

- Tear secretion kinetics

- Schirmer test

- Schirmer-Holly test

- dye-dilution test [6]

- tear meniscus assessment

- tear thinning time [7]

- lacrimal equilibration time [8]

- osmolality

- mucus ferning

- tear cytology

- protein content

- lactoferrin concentration (Lactoplate®)

- enzymatic activity

Tear Film Related:

- tear film break-up time (T-BUT)

- fluorescein T-BUT

- non-invasive optical T-BUT [9, 10, 11]

- tear evaporation rate

- lipid spreading ability

Ocular Surface Related:

- vital staining

- Rose Bengal

- Fluorescein

- 1% Lissamine Green

    - similar specificity as Rose Bengal

- surface cytology

- impression cytology

- surface microscopy (specular reflection microscopy)

BIBLIOGRAPHY

1.   Holly F. Diagnostic Methods on Treatment Modalities of Dry Eye Conditions. International Ophthalmology 1993;17:113-25.

2.   Schwartz CA. Specialty Contact lenses: A Fitter's Guide. 1st ed, Philadelphia, London, Toronto, Montreal, Sydney, Tokyo: WB Saunders Company, 1996.

3.   Bjerrum K. Test and Symptoms in Keratoconjunctivitis Sicca and their Correlation. ACTA Ophthalmol Scand 1996;74:436-41.

4.   Lemp M. Report of the National Eye Institute/Industry Workshop on Clinical Trials in Dry Eyes. CLAO 1995;21:221-32.

5.   Toda I, Fujishima H, Tsubota K. Ocular Fatigue is the Major Symptom of Dry Eye. ACTA Ophthalmologica 1993;71:347-52.

6.   Mishima S, Gasset T, Klyce SJ, Baum J. Determination of tear volume and tear flow. Investigative Ophthalmology 1966;265-76.

7.   Patel S, Farrell J, Bevan R. Relation between Precorneal Tear Film Stability and Tear Production Rate in Normal Eyes. Optometry and Vision Science 1989;66:300-3.

8.   Lavaux J, Keller W. Lacrimal Equilibration Time (LET): A Quick and Simple Dry Eye Test. Optometry and Vision Science 1993;70:832-8.

9.   Cho P, Douthwaite W. The Relation between Invasive and Noninvasive Tear Break-up Time. Optometry and Vision Science 1995;72:17-22.

10.   Brown B, Cho P, Yap M. Mechanical manipulation of the lids and tear break-up time measurements in Hong Kong Chinese. Ophthal Physiol Opt 1993;1993:233-8.

11.   Norn M. Tear Film Break-Up Time. A Review. In: Holly FJ, ed. The Preocular Tear Film In Health, Disease, and Contact Lens Wear, Lubbock TX: Dry Eye Institute, Inc, 1986:52-6.

APPENDIX 2

Image Processing Protocol

Various imaging systems and techniques were evaluated for use in this study [1]. The spatial frequency content of sample images from a standard fundus camera, stereo-fundus camera, and video biomicroscope were evaluated. Surprisingly, the spatial content in all formats was less than three cycles/degree. Therefore, direct comparison of fundus detail frequencies to standard visual acuity (frequencies) was limited. The application of these techniques to recent super high resolution imaging (imaging of retinal cells: rods and cones) was not attempted. Because of similarity between image detail information derived from these standard systems, video biomicroscope imaging was selected to enable continuous real-time data acquisition. For this study all fundus image data were collected and recorded on high definition video tape (S-VHS). The mechanisms used for data collection are described below.

IMAGE CAPTURE:

The video recording system utilized a high resolution CCD video camera (Sony DXC-107AP) attached to a standard biomicroscope (Zeiss Video Slit lamp, model 20 SL). The output from the CCD video camera was captured on high definition S-VHS video recorder (Mitsubishi HS-U69).

Image magnification was accomplished by standard biomicroscope control and by the +90 Diopter Volk fundus lens. The biomicroscope magnification was determined to be optimal at 20x. Prior testing of system parameters found greater magnification

47

resulted in decreased image intensity. To overcome this decrease image intensity, the required increase in illumination created subject discomfort and reflexive tearing. Reduced magnification reduced the pixel (picture elements) resolution of the retinal vessel. Subsequent digitization of these lower magnification images resulted in some retinal vessel profiles that were represented by one to five pixels. Using this study's selection of 20x, typical retinal vessel profiles were represented by 10 to 20 pixels.

The CCD video camera captures a real fundus image from the biomicroscope / +90 Diopter system in a 752 x 582 pixel array. This array is output to and recorded at 30 frames / second (standard NTSC signal) on an analog S-VHS video recorder (Mitsubishi HS-U69). The standard NTSC protocol dictates a video image resolution to be 720 x 486 pixels.

IMAGE DIGITIZATION:

The video image information captured was imported by the standard video input (S-VHS) provided on Apple Power Macintosh 7500/100. This system allows for high speed analog to digital conversion of standard video format. The digitization of the fundus video images was controlled by a video processing program (Avid VideoShop® 3.0.2). The maximum array allowed by this program was 640 x 480 pixels with a gray scale of 256. This has reported to be more than adequate for valid image representation[1]. Sequential digitized video images were accomplished for all trials using this maximum allowable array size at one frame / second.

IMAGE PROCESSING:

Due to normal eye saccades and momentary fixation losses over the acquisition time, retinal images required alignment corrections. To minimize the impact of small eye movements during acquisition, alignment errors were verified and compensated in each image of a series. This and subsequent processing was accomplished using NIH-Image (version 1.60; http://rsb.info.nih.gov/nih-image/). Appendix 3 contains a series of macros created and used in conjunction with NIH-Image. Vessel intensity profiles (figure 1) were developed for three vessel locations in each series. These intensity profiles were collated and examined in Excel (version 5.0; Microsoft Corp.) Local vessel contrast values were determined by Weber's definition "(delta L)/L" for each location over the series. The vessel contrast values for the three locations were then averaged and normalized for comparison to other vessel and psychophysical data.

<div align="center">BIBLIOGRAPHY</div>

1.   Gilchrist J. Computer Processing of Ocular Photographs - A Review. Ophthal Physio Opt 1987;7:379-80.

APPENDIX 3

<u>NIH-Image: Visual Alignment/Analysis Macros</u>

This is a set of macros for aligning pictures in a stack with manual assistance and other miscellaneous functions. This series of macros were designed for use with the NIH-Image program(version 1.60). NIH-Image, source code, example macros and plugins are available from the NIH Image Web site (http://rsb.info.nih.gov/nih-image/) or by anonymous FTP from zippy.nimh.nih.gov.

PROTOCOL FOR IMAGE ALIGNMENT:

Select the image to be used for reference   ([R] - Reference Image, default = 1st image)

Select the image to be aligned   ([N]   Next Image {advance}   )

                                                     ([B]   Back one Image (return }   )

                                                     ([G]   Goto Image {jump to selected}   )

Flicker to visually compare alignment   ([F]   Flicker Images {oscillate images})

Press "control" key to stop flicker   ("Ctrl" on keyboard   )

Use the arrow keys to move the image   (← ↑ → ↓ on keyboard   )

Repeat steps to confirm alignment

Repeat steps and/or for each image in series

====== Written by ======

Ronald C. Tutt, OD, Indiana University, Physiological Optics

Comments and bug reports to: *tutt @ alaoc.brooks.af.mil*

Version 1.2, last modified 6 Jan 97

Requires Image version 1.60

==== List of Macros ====

MISCELLANEOUS MACROS

[+] Add Image   {Adds image to stack}

[-] Delete Image   {Deletes current image from stack}

[*] Insert Duplicate Image   {Insert copy of current image in the stack}

[1] Sharpen   {Image filter}

[2] Smooth   {Image filter}

[3] Reduce Noise   {Image filter}

[4] Invert Image Scale   {Inverts Image Scale for all images in the stack}

[5] Crop Images   {Crops stack to ROI dimensions, deletes old stack}

[6] Generate FFT of this Stack   {Generates Fast Fourier Transform}

[7] Subtract Image BKG   {Image filter}

[8] Double Stack Image   {Converts two stacks into 1 double image stack}

VISUAL ALIGNMENT MACROS

[F] Flicker Images   {Flicker reference image with current image}

[R] Reference Image   {Select reference image (default = 1st image)}

[N] Next Image   {Advance to next image}

[B] Back one Image   {Return to previous image}

[G] Goto Image   {Jump to selected image}

STACK DISPLAY AND DATA MACROS

[P] Create sequential Profiles   {Create profile data from line or rectangle ROI}

[A] Animate Stack   {Display stack as a movie}

[S] Sequential descriptive data   {Create descriptive data from ROI over stack}

{ global variables }

var

  Saln,Sref:integer;   {Image Locators for reference and Alignment images }

  Stmp:integer;   {Temporary image pointer }

  reflength,refangle:real;   { distance and angle from point 1 to point 2 }

macro '   STACK PROCESSING'; begin end;

macro '(-'; begin end;

procedure Error(s:string);   { Error and CheckForStack are utility routines. }

   begin   {Error(s) issues the error message S and terminates the macro. }

    PutMessage(s); exit;

   end;

procedure CheckForStack;

   begin

52

```
    if nSlices=0 then Error ('This window is not a stack');

  end;



{ MACROS}

macro '[+]    Add Image';              begin AddImage end;

macro '[-]    Delete Image';           begin DeleteImage end;

macro '[*]    Insert duplicate Image';

   begin

     CheckForStack;

     SelectAll; Copy;

     AddSlice; Paste;

     Saln:=Slicenumber

   end;



macro '(-' begin end;                  {draw a line between sections}



macro '[1]    Sharpen';                {Image filter}

var

  i:integer;

begin

  CheckForStack;

  for i:= 1 to nSlices do begin

    SelectSlice(i);
```

```
    SetOption; Smooth;

    SetOption; Sharpen;

  end;

end;


macro '[2]    Smooth';                    {Image filter}

var

  i:integer;

begin

  CheckForStack;

  for i:= 1 to nSlices do begin

    SelectSlice(i);

    SetOption; Smooth;

  end;

end;


macro '[3]    Reduce Noise';              {Image filter}

var

  i:integer;

begin

  CheckForStack;

  for i:= 1 to nSlices do begin

    SelectSlice(i);
```

```
        ReduceNoise;

    end;

end;


macro '[4]    Invert image scale';        {Image filter}

    var i,s:integer;

        begin

            If (nSlices=0) then Invert else begin

            s:=SliceNumber;

                For i:=1 to nSlices do begin

                ChooseSlice(i); Invert;

                    end;

            SelectSlice(s);

                end;

            end;


macro '[5]    Crop Images to ROI dimensions';

var

    l,t,w,h,n,old,new,i:integer;

    wt:string;

    begin

        CheckForStack;

            n:=nSlices; old:=PicNumber; wt:=WindowTitle;
```

```
   GetRoi(l,t,w,h);

      if (w <=0) then begin                    { default is to shrink by 50 }

         GetPicSize(w,h);

         l:=50; t:=50; w:=w-100; h:=h-100;

      end;

   SetNewSize(w,h);

   MakeNewStack('Cropped ',wt);

   new:=PicNumber;

 for i:=1 to n do begin

   ChoosePic(old); ChooseSlice(1);

   MakeRoi(l,t,w,h); Copy; DeleteSlice;

   ChoosePic(new); ChooseSlice(i); Paste;

   if (i<n) then AddSlice;

 end;

   ChoosePic(old); Dispose;

   SelectPic(new-1);

 end;


macro '[6]   Generate FFT amplitude images';         {Image filter}

var

 l,t,w,h,n,old,new,i:integer;

 wt:string;

 begin
```

```
CheckForStack;

    n:=nSlices; old:=PicNumber; wt:=WindowTitle;

    GetPicSize(w,h);        { get current picture size}

   SetNewSize(w,h);            {Set new window size the same as old}

   MakeNewStack('FFT (Forward)',wt);   {create a new stack to store images}

   new:=PicNumber;

 for i:=1 to n do begin

  ChoosePic(old); ChooseSlice(i);

  FFT('foreward'); SelectAll; Copy; Dispose;NextWindow;

  ChooseSlice(i); Paste;

 end;

end;


macro '[7]    Subtract BKG {2D rolling ball}';         {Image filter}
var
 radius,i:integer;
begin
 CheckForStack;
 radius:=GetNumber('Rolling ball radius (pixels):',50);
 for i:= 1 to nSlices do begin
  SelectSlice(i);
  SubtractBackground('2D Rolling Ball',radius);
 end;
```

end;

macro '[8]   Converts 2 stacks into 1 double image stack;

{Combines two stacks(w1xh1xd1 and w2xh2xd2) to create

a new w1+w2 x max(h1,h2) x max(d1,d2) stack. For

example, a 256x256x40 and a 256x256x30 stack would be

combined into one 512x256x40 stack.}

var

i,w1,w2,w3,h1,h2,h3,d1,d2,d3:integer;

begin

SaveState;

if nPics<>2 then begin

PutMessage('This macro operates on exactly two stacks.');

exit;

end;

SelectPic(1);

GetPicSize(w1,h1);

d1:=nSlices;

SelectPic(2);

GetPicSize(w2,h2);

d2:=nSlices;

if d1>=d2

then d3:=d1

```
  else d3:=d2;

if d3=0 then begin

  PutMessage('Both images must be stacks.');

  exit;

end;

w3:=w1+w2;

if h1>=h2

  then h3:=h1

  else h3:=h2;

SetNewSize(w3,h3);

MakeNewStack('Double Image Stack');

for i:=1 to d3 do begin

  SelectPic(1);

  SelectSlice(1);

  SelectAll;

  Copy;

  DeleteSlice;

  SelectPic(3);

  MakeRoi(0,0,w1,h1);

  Paste;

  SelectPic(2);

  SelectSlice(1);

  SelectAll;
```

```
Copy;

DeleteSlice;

SelectPic(3);

MakeRoi(w1,0,w2,h2);

Paste;

if i<d3 then AddSlice;

end;

SelectPic(1);

Dispose;

SelectPic(1);

Dispose;

RestoreState;

end;

end;
```

```
macro '(-'; begin end;                      {draw a line between sections}

macro '      VISUAL ALIGNMENT'; begin end;

macro '(-'; begin end;                      {draw a line between sections}


macro '[F]   Flicker Images';               { Image Flick routine}

   begin

       if(Sref=0) Then Sref := 1;           {default reference slice is image #1}

       Saln:=SliceNumber ;                  {Start with current slice}
```

```
KillRoi;                              {Clear current ROI, if selected}

Selectslice(Saln);                    {Select  slice for alignment}

SelectAll;                            {Draw new ROI (full image) }

 Copy;                                {Copy alignment slice}

 KillRoi;                             {clear ROI}

 Paste;                {paste alignment image (this allows movement with arrows}

showmessage('Press CONTROL key to exit Flicker');

 Repeat                               {Flicker loop}

   selectslice(Sref);                 {Select  reference slice}

   selectslice(Saln);                 {Select  slice for alignment}

 Until KeyDown('control');            {Repeat until mouse button is clicked}

    paste;                            {Paste alignment image as aligned}

end;



macro '[R]    Set Reference Image';       {choose image for Flicker reference}

  begin

   CheckForStack;

   if(Sref=0) Then Sref := 1;             {default reference slice is image #1}

    Repeat

       Sref:=GetNumber('Use Reference Image # :', Sref,0);

      Until (Sref<=nSlices);

   end;
```

```
macro '(-' begin end;                    {draw a line between sections}


macro '[N]   Next  image';               {advance to next image}
var

   s:integer;

  begin

   CheckForStack;

   SaIn:=SliceNumber ;                   {Start with current slice}

      SaIn := SaIn + 1;                  {increment to next image}

      If(SaIn>nSlices) then SaIn := 1;   {wrap to first image}

    SelectSlice(SaIn);

  end;



macro '[B]   Previous Image';            {return to previous image}
var

   s:integer;

  begin

   CheckForStack;

   SaIn:=SliceNumber ;                   {Start with current slice}

      SaIn := SaIn - 1;                  {increment to next image}

      If(SaIn<1) then SaIn := nSlices;   {wrap to last image}

    SelectSlice(SaIn);

  end;
```

```
macro '[G]    Go to Image';                    {jump to selected image}

  begin

    CheckForStack;

    if(Saln=0) Then Saln := 1;    {default Alignment Slice is image #2}

      Repeat

        Saln:=GetNumber('Enter which Slice to align:', 1);

        Until (Saln<=nSlices);

      SelectSlice(Saln);

    end;


macro '(-'; begin end;

macro '        STACK DISPLAY & DATA'; begin end;

macro '(-'; begin end;


macro '[P]    Create sequential Profiles from ROI';

var

  l,t,w,h,s,i,j,k:integer;

   count, ppv, ymin, ymax, i: integer;

   scale: real;

   unit: string;

  begin

    CheckForStack;
```

```
    k := SliceNumber;  {save current slice image #}

    GetROI(l,t,w,h);

        if (w=0) then begin

        Error('a ROI must be drawn for profiles.');

        end;



NewTextWindow('Plot Values', 150, 250);

    { writeln('                          ');}

    s:=nSlices+1;

        For i:=1 to nSlices do begin

        s:=s-1;

    Showmessage ('Remaining  slices to process: ',s);

        ChooseSlice(i);

            GetPlotData(count, ppv, ymin, ymax);

                for j:= 0 to count -1 do

                write(PlotData[j]:1:0,'      ');

                writeln('Slice Data ',i,'      ');

            end;

    Selectslice(k);   {Reset to original slice display}

end;



 macro '[A]    Animate Stack';                    {display like a movie}

var
```

```
  i,icnt,delay:integer;

begin

 RequiresVersion(1.56);

 CheckForStack;

i:=0;

icnt:=0;

 delay:=0.1;

 repeat

  i:=i+1;

  if i>nSlices then i:=1;

  Wait(delay);

  SelectSlice(i);

  if KeyDown('shift') then delay:=1.5*delay;

  if delay>1 then delay:=1;

  if KeyDown('control') then delay:=0.66*delay;

  if KeyDown('option') then beep;

  if icnt=5 then ShowMessage('decrease delay = "shift"\increase delay  = "control"\Click

on image to end\delay=',delay:4:2);

  icnt:=icnt+1;

  if icnt>5 then icnt:=0;

 until button;

end;

 ShowMessage('delay=',delay:4:2);
```

```
end;


macro '[S]  Sequential descriptive measures from ROI';  {display size,max, min, avg,etc}
var
 l,t,w,h,s,i,j,k:integer;
  count, ppv, ymin, ymax, i: integer;
  scale: real;
  unit: string;
 begin
    CheckForStack;
   k := SliceNumber;  {save current slice image #}
   GetROI(l,t,w,h);
     if (w=0) then begin
     Error('a ROI must be drawn for profiles.');
     end;


NewTextWindow('Measure Values', 150, 250);
   write('Mean','               ','Std Dev','     ',' Min','       ','Max','        ');
   writeln(' ');
   s:=nSlices+1;
     For i:=1 to nSlices do begin
     s:=s-1;
   Showmessage ('Remaining  slices to process: ',s);
```

```
ChooseSlice(i);

  Measure;

    write(' ',rMean[i]:8:3,' ',rStdDev[i]:8:3,'',rMin[i]:8:3,'  ',rMax[i]:8:3,'');

    writeln('Slice Data ',i,' ');

  Selectslice(k);   {Reset to original slice display}

end;
```

End Of Macro Listing

VITAE

Ronald Cogswell Tutt was born on the 25th of February 1954 in Alliance, Nebraska. He graduated from Alliance High School in 1972 and attended the University of Nebraska - Lincoln for pre-medical education. He received Associate of Science and Bachelor of Science degrees in Nuclear Medicine Technology in 1977 from the University of Nebraska Medical Center. He attended Pacific University College of Optometry, Oregon and was granted Doctor of Optometry in 1988. In March 1988, he earned direct commission in the United States Air Force Biomedical Science Corps.

As an Air Force Optometry Officer, he held the following positions:

OIC, Contact Lens Services	1988-1990	Randolph AFB, Texas
Deputy Chief, Optometry Services	1990-1992	Kadena AB, Japan
Chief, Optometry Services	1992-1995	Kadena AB, Japan
Post Graduate Student (Physiological Optics)	1995-1997	Indiana University Bloomington, Indiana
Chief, Contact Lens Research	1997-1998	Brooks AFB, TX
Chief, Aeromedical Research	1998-Present	Brooks AFB, TX

During his military career he was awarded the Biomedical Science Corps Senior badge, the Air Force Commendation Medal, and the Meritorious Service Medal. He graduated from Squadron Officers School and Air Command & Staff College. In

addition he holds certification in Advanced Trauma Life Support and Pediatric Advance

Life Support. He presently holds the rank of Major.

He is a member of the Armed Forces Optometric Society, American Optometric

Association, and a student member of the American Academy of Optometry. He is also a

member of the Beta Sigma Kappa Honor Fraternity and Air Force Association.